

Johannes Mauhart, Bsc

**Resonance Assignment and 3D Structure Calculation of the  
Transmembrane Domain of ToxR and Improvements to the  
Slice-Selective Instant Homonuclear Decoupling Pulse Sequence**

**MASTER'S THESIS**

to achieve the university degree of

Master of Science

Master's degree programme: Chemistry

submitted to

**Graz University of Technology**

Supervisor

Ao.Univ.-Prof. Mag. Dr.rer.nat. Klaus Zangger

Institute of Chemistry

NAWI Graz


Graz, June 2015

## AFFIDAVIT

I declare that I have authored this thesis independently, that I have not used other than the declared sources/resources, and that I have explicitly indicated all material which has been quoted either literally or by content from the sources used. The text document uploaded to TUGRAZonline is identical to the present master's thesis dissertation.

17.06.2015

Date



Signature

People love chopping wood.  
In this activity one immediately sees results.

*Albert Einstein*

## Acknowledgements

In the beginning I want to thank Prof. Klaus Zangger for supervising and supporting me during my master thesis. It was not easy all the time, but in the end I learned a lot about structural biology and NMR spectroscopy. He really shines when it comes to theoretical and practical aspects of NMR spectroscopy.

I was assigned to several different projects, many of which didn't work out the right way. Nevertheless it was a lesson that I am grateful of having had.

I want to thank all the people from the AG Zangger, who supported me during my thesis. I want to thank Nina, Bernd and Simon for having an open ear, when I needed to talk something off my mind over a hot or cold beverage. And I want to thank Gabriel for teaching me a lot of molecular biology techniques, even though I sometimes might have taken longer paths to reach a goal than necessary. Special thanks goes to Evi for the nice conversations and for proofreading the greater part of my thesis.

Thanks to my parents, for supporting me during my study and my brother and sister for being there for me together with my parents at home in Upper Austria.

I want to thank my friends, especially Mathias who was a constant companion during my study, Daniel for showing me the beauty of the mountains and constantly motivating me to keep going. I also want to thank Christian, Sabrina, Stefan, Benjamin and Eva for having a good time altogether. Peter, Mapi, Luki and the other members of the gang also deserve thanks for unforgettable evenings and all the incredible stuff we did. Additional thanks go to my friends Philipp and Thomas back at home in Upper Austria for being there for me when I am at home.

# Contents

<b>1</b>	<b>The transmembrane domain of ToxR</b>	<b>1</b>
1.1	Introduction . . . . .	1
1.1.1	<i>Vibrio cholerae</i> and cholera disease . . . . .	1
1.1.2	The Virulence Cascade in <i>V. cholerae</i> . . . . .	1
1.1.3	The Transmembrane Transcription Factors ToxR, ToxS, TcpP and TcpH . . . . .	1
1.1.4	Environmental Signals and Gene Control . . . . .	3
1.1.5	Structure of ToxR . . . . .	3
1.2	Methods . . . . .	3
1.2.1	Sequence Analysis . . . . .	3
1.2.2	Data Aquisition . . . . .	4
1.2.3	Chemical Shift Assignment . . . . .	5
1.2.4	Structure Calculation . . . . .	6
1.2.5	Unlabelled Protein Expression . . . . .	6
1.2.6	SDS Polyacrylamide Gel Electrophoresis . . . . .	7
1.2.7	Protein Purification . . . . .	8
1.2.8	TEV Cleavage . . . . .	9
1.2.9	Mass Spectrometry . . . . .	10
1.2.10	Preparation of Samples for NMR Spectroscopy . . . . .	10
1.2.11	NMR Spectroscopy . . . . .	11
1.3	Discussion . . . . .	12
<b>2</b>	<b>Improvements to the Slice-Selective Instant Homonuclear Decoupling</b>	<b>13</b>
2.1	Introduction . . . . .	13
2.1.1	Slice-Selective Instant Homonuclear Broadband Decoupling . . . . .	13
2.1.2	Bilinear Rotational Decoupling . . . . .	14
2.1.3	PSYCHE . . . . .	15
2.2	Methods . . . . .	16
2.2.1	Artifact Suppression by using a Variable Data Chunk Lengths . . . . .	16
2.2.2	Shorter Acquisition Times by Relaxation Delay Reduction using Frequency Shifted Pulses . . . . .	17
2.3	Discussion . . . . .	20
<b>3</b>	<b>Appendix</b>	<b>21</b>
3.1	Materials . . . . .	21
3.1.1	Bacterial Strains, Enzymes, Kits and Plasmids . . . . .	21
3.1.2	Media and Stocks . . . . .	21
3.1.3	Buffers . . . . .	22
3.2	Data . . . . .	23
3.2.1	Sequences . . . . .	23
3.2.2	Mass Spectroscopy Spectra . . . . .	23
3.2.3	Pulse Sequences . . . . .	25
3.2.4	Shape Lists . . . . .	28
3.2.5	Delay List . . . . .	28
3.3	List of Acronyms . . . . .	29
3.4	References . . . . .	29

# 1 The transmembrane domain of ToxR

## 1.1 Introduction

### 1.1.1 *Vibrio cholerae* and cholera disease

*V. cholerae* is a Gram-negative, motile, comma shaped, facultative anaerobic bacterium.<sup>[1, 2]</sup> It prevails in aquatic environments forming biofilms on surfaces like planktons.<sup>[3]</sup> The pathogenic strains O1 Classic, O1 El Tor and O139 are able to survive in the human small intestine after oral uptake of contaminated water and attach themselves to epithelial cells utilizing the toxin-coregulated pilus (TCP).<sup>[4]</sup> Cholera toxin (CT) is an AB<sub>5</sub>-type protein complex, and becomes active after the extracellular hemagglutinin/protease cleaves subunit A into two parts that are still connected by a disulfide bridge.<sup>[5]</sup> The active part of subunit A then facilitates increased cyclic-AMP production, causing massive diarrhea, the main symptom of cholera.<sup>[6]</sup>

### 1.1.2 The Virulence Cascade in *V. cholerae*

The expression of the virulence factors CT and TCP is dependent on the activation of their respective genes (*ctx* and *tcp*) by the ToxT protein.<sup>[6]</sup> ToxT also enhances the transcription of the accessory colonization factor genes *acfA-D* and the *aldA* gene encoding aldehyde dehydrogenase.<sup>[7]</sup> Binding of ToxT to *ctxAB* and *tcpA* competes with the histone-like nucleoid structuring protein (H-NS), a global prokaryotic gene regulator, which represses transcription.<sup>[8, 9]</sup> ToxT expression is regulated by the two membrane bound protein complexes TcpPH and ToxRS transcriptionally activating *toxT*,<sup>[10–12]</sup> which is repressed by H-NS and also influenced by citric acid cycle intermediates.<sup>[9, 13]</sup>

*tcpPH* transcription is facilitated by the proteins AphA, AphB and repressed by the phosphate regulation associated protein PhoB,<sup>[14–17]</sup> whereas transcription of *toxRS* is enhanced by AphB.<sup>[18]</sup>

HapR is a regulatory protein, with *hapR*-mRNA being destabilized at low cell density, involved in downregulating biofilm formation and virulence gene expression via repression of *aphA* transcription.<sup>[19, 20]</sup> This is part of a process called "mucosal escape response".<sup>[21, 22]</sup>

Cyclo(Phe-Pro) (cFP) has been shown to inhibit virulence factor production by activating the transcription of *leuO* through ToxR and LeuO represses transcription of *aphA*.<sup>[23]</sup>

Capsaicin enhances the expression of H-NS, which blocks transcription of the *toxT*, *ctxAB* and *tcpA* genes.<sup>[24, 25]</sup> For a graphical representation of the virulence cascade see Figure 1.1.

### 1.1.3 The Transmembrane Transcription Factors ToxR, ToxS, TcpP and TcpH

Additionally to the activation of *toxT*, ToxR is involved in the transcription regulation of the outer membrane porin (*omp*) genes *ompU* and *ompT*,<sup>[26]</sup> with the transcription of *ompU* being regulated positively and the transcription of *ompT* negatively, but both being dependent on the dsbAB system, which controls the disulfide bond formation in ToxR.<sup>[27]</sup>

Disulfide bonds play a key role in the regulation of virulence factor expression, as components of bile lead to homodimerization of TcpP, which is a transmembrane protein like ToxR, via disulfide bond formation in the periplasmic domain, by this enhancing virulence gene transcription. The intramolecular disulfide bridge present in the absence of bile was shown to have an inhibitory effect on virulence gene transcription.<sup>[28]</sup>

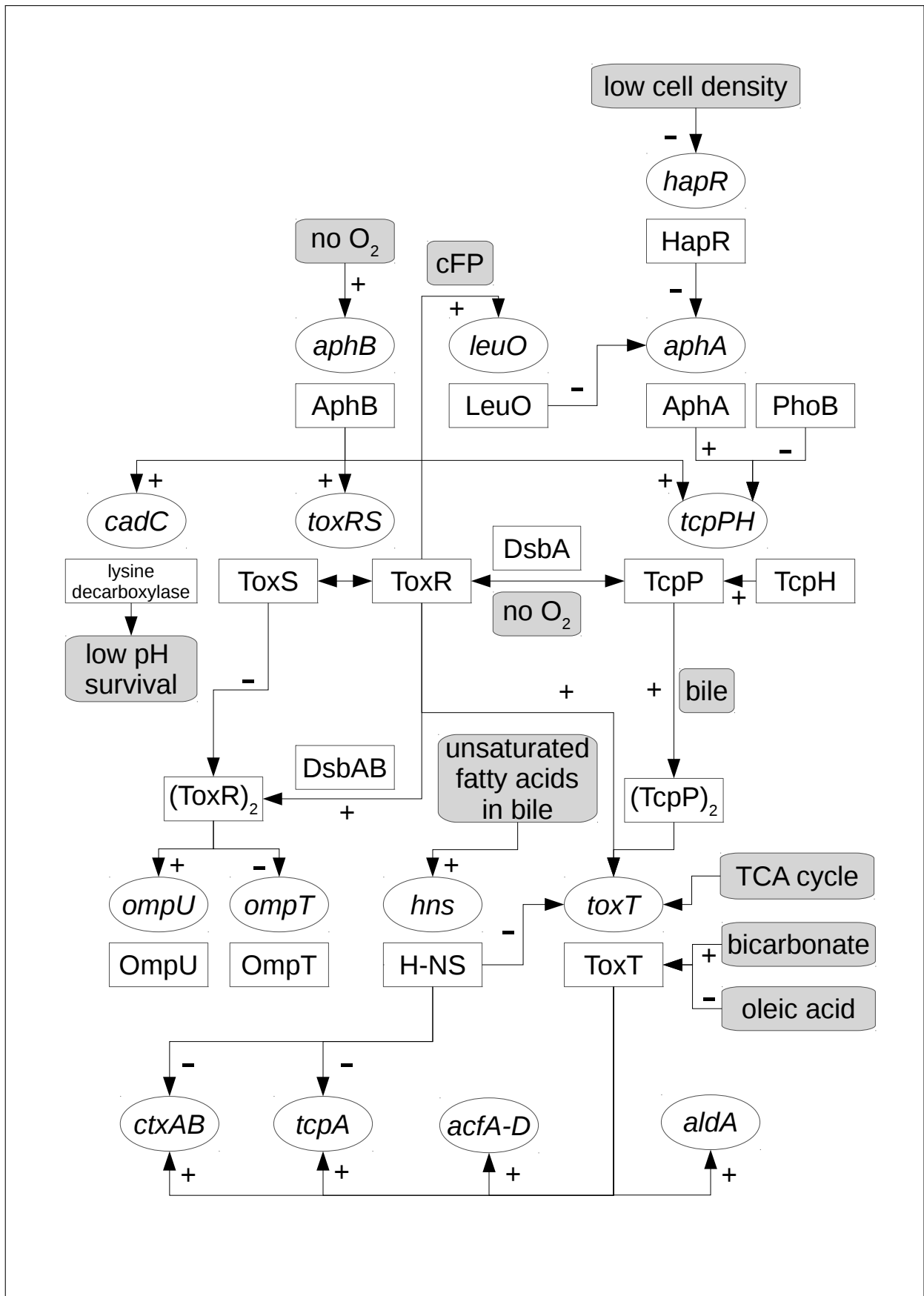


Figure 1.1: Overview of the *V. cholerae* virulence cascade

ToxS and TcpH are membrane localized proteins consisting of a short membrane anchor and a larger periplasmic domain. TcpH has been shown to block degradation of TcpP, and levels of ToxR to be independent of the presence of ToxS,<sup>[29]</sup> additionally ToxS blocks the homodimerization of ToxR.<sup>[27]</sup>

### 1.1.4 Environmental Signals and Gene Control

Bile affects the porin OmpT, by reducing its flux in the presence of bile, though bile does not influence the flux of the porin OmpU, which is the dominantly expressed porin of the two under virulence inducing conditions.<sup>[30]</sup> This might explain the resistance of *V. cholerae* to bile and anionic detergents. Presence of OmpU is also correlated with *toxT* transcription,<sup>[31]</sup> explaining the importance of bile tolerance to the homodimerization of TcpP, which regulates *toxT* transcription. In classical *V. cholerae* strains bile also enables direct activation of the *ctxAB* promoter by ToxR.<sup>[32]</sup>

The unsaturated fatty acids present in bile suppress transcription of *ctxAB* and *tcpA* with H-NS by competing with ToxT and also increase the motility of *V. cholerae*. Cholesterol also enhances motility independently of H-NS, ToxR and ToxT.<sup>[33]</sup> The crystal structure of ToxT indicates that oleic acid negatively influences the expression of TCP and CT.<sup>[34]</sup> Bicarbonate is a positive effector for ToxT.<sup>[35]</sup>

Induction of TcpP expression by AphB<sup>[36]</sup> under anaerobic conditions is governed by the reversible cysteine switch.<sup>[37]</sup> AphB is also responsible for expression of *cadC* decoding lysine decarboxylase, which is beneficial to survival at low pH.<sup>[38]</sup>

Anaerobiosis also enhances the expression of six proteins involved in the pathogenesis of the *V. cholerae* El Tor strain and leads to an interaction between ToxR and TcpP.<sup>[39, 40]</sup>

### 1.1.5 Structure of ToxR

The ToxR protein consists of three subunits: the cytoplasmic domain containing a DNA binding motif, the transmembrane domain and the periplasmic domain, which contains two cysteines with C236 being buried and C293 creating interchain disulfide bridges to form homodimers.<sup>[41]</sup> The periplasmic domain of ToxS has been shown to interact with the periplasmic domain of ToxR *in vitro* by forming a complex independent of its oxidation state.<sup>[42]</sup> Furthermore, the presence of ToxS prevents ToxR homodimers formation.<sup>[27]</sup> Structural studies of the cytoplasmic domain showed the winged Helix Turn Helix DNA binding motif (wHTH), which is commonly found in membrane bound transcription activators.<sup>[43]</sup>

## 1.2 Methods

### 1.2.1 Sequence Analysis

This project attempted to unravel the structure and structure associated properties of the transmembrane domain of ToxR (tm-ToxR) for full functionality of ToxR. To identify the transmembrane domain within the sequence of ToxR<sup>[44]</sup> the program tmpred<sup>[45]</sup> was used (see Figures 1.2 and 1.3). Although the score varies depending on the direction of the membrane insertion, the sequence spanning the membrane is the same. The peptide representing tm-ToxR (see Appendix 3.2.1, Table 3.5) was purchased from Pepnome, Hongkong, China. A peptide containing the amino acid substitution P15A was ordered, to investigate the importance of proline in this helix, but it could not be synthesized by the manufacturer.

The vectors pETMBP and pETZ2 with tm-ToxR used for recombinant expression of tm-ToxR with the solubility tags Maltose Binding Protein (MBP) and IgG binding domain (Z-domain) of *Staphylococcus aureus* protein A (Z2), contained a slightly different part of tm-ToxR (see Appendix 3.1.1, Table 3.5).



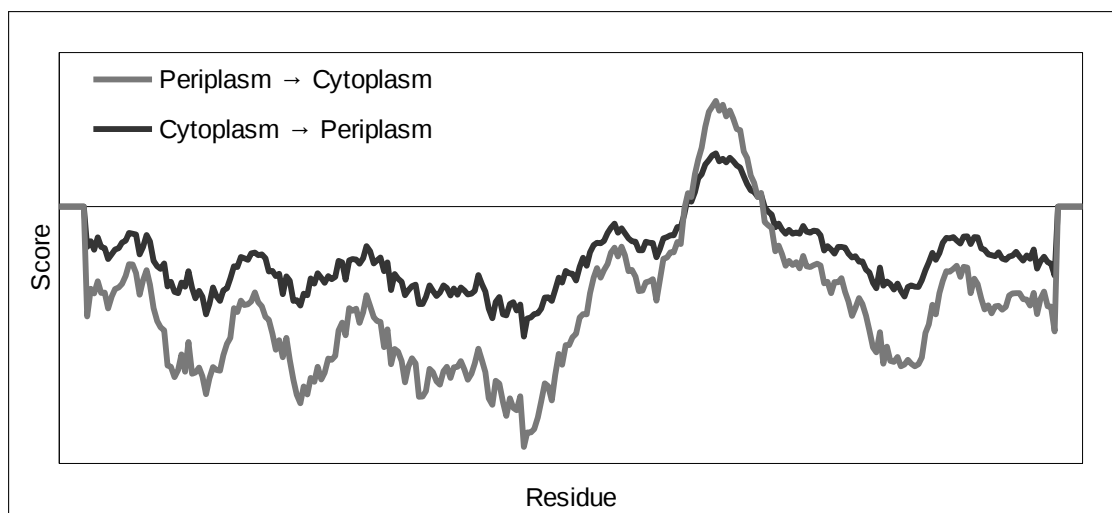


Figure 1.2: Result from tmpred for the sequence of ToxR (see Appendix 3.2.1, Table 3.4) featuring a score for both directions of membrane insertion, and the horizontal line separating positive and negative scores

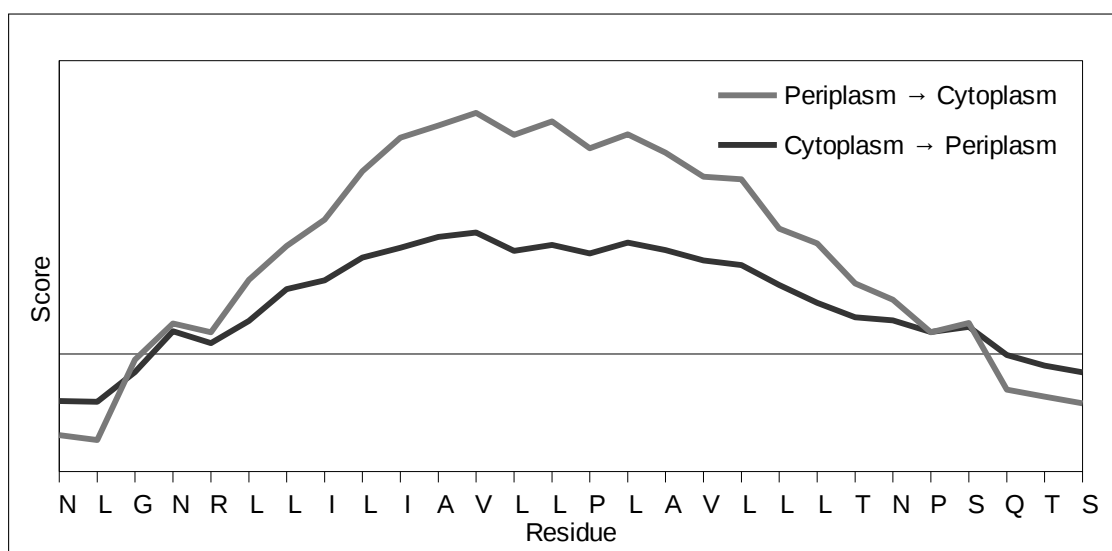


Figure 1.3: Enlarged transmembrane part from the tmpred result with designated amino acids

### 1.2.2 Data Acquisition

$^1\text{H}$  spectra of the following samples (summarized in Table 1.1) were acquired on a Bruker Avance DRX 500 MHz NMR spectrometer equipped with a Triple-Resonance Probe at 300 K and evaluated regarding the number of sharp peaks appearing in the amide,  $\text{C}_\alpha$ , and side-chain proton regions. A high number of sharp peaks (see Figure 1.4) corresponds to a better defined structure of the peptide in the sample.

The spectra of Samples 1-5 were quite similar independently of the concentration and type of micelles and lacked a high number of sharp peaks. The spectrum of Sample 6 indicated a better defined structure of the peptide. Therefore Sample 6 was used to acquire the following 2D spectra required for chemical shift assignment of the peptide (see Table 1.2).

A solvent suppression scheme was employed during the Total Correlation Spectroscopy (TOCSY) and Nuclear Overhauser Enhancement Spectroscopy (NOESY) experiments to suppress the broad

Table 1.1: List of prepared and measured samples

No.	System	Volume [ $\mu\text{L}$ ]	Peptide		Detergent		Micelles [mM]	Micelles/Peptide
			[mg]	[mM]	[mg]	[mM]		
1	dDPC in Buffer 1	600	1.4	0.95	11.7	55	0.79	1.20
2	dDPC in Buffer 1	650	1.4	0.88	23.5	103	1.47	1.67
3	dDPC in Buffer 1	700	1.4	0.82	35.3	143	2.05	2.51
4	dSDS in Buffer 1	600	1.0	0.68	18.6	107	1.34	1.91
5	dSDS in Buffer 1	650	1.0	0.62	40.8	218	2.72	4.37
6	d <sub>2</sub> -TFE	600	1.0	0.68				

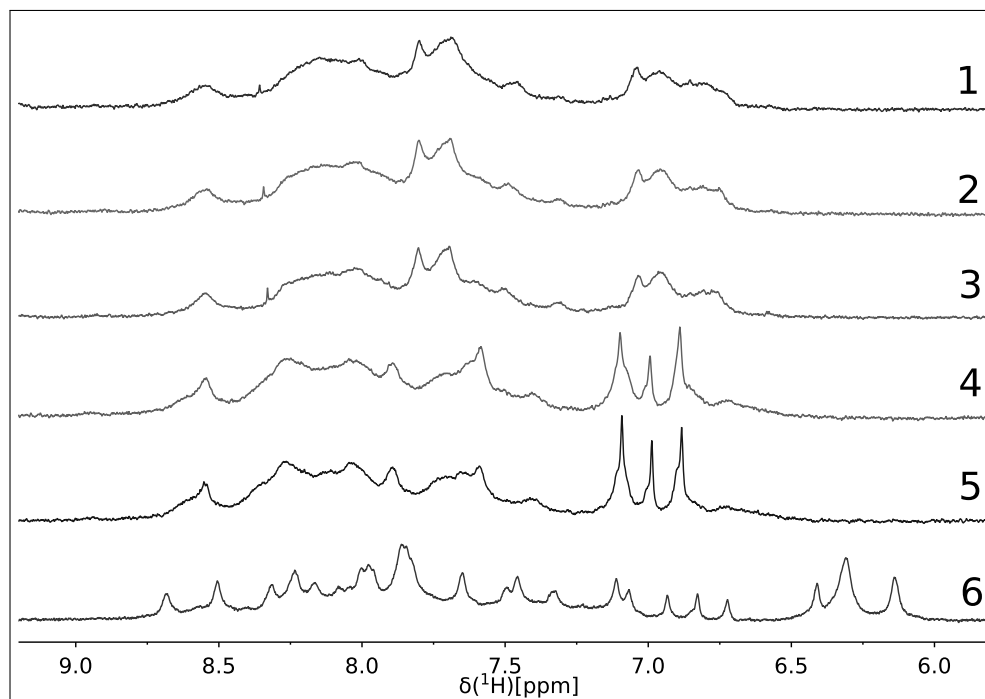


Figure 1.4: NH part of 1D spectra of Samples 1-6

OH proton resonance of deuterated 2,2,2-Trifluoro ethanol (d<sub>2</sub>-TFE). As the peptide was not isotopically labelled, long acquisition times were required for the Heteronuclear Single Quantum Correlation (HSQC) experiments. All spectra were processed using NMRPipe.<sup>[47]</sup>

### 1.2.3 Chemical Shift Assignment

The chemical shift assignment was done utilizing amino acid chemical shift databases,<sup>[48, 49]</sup> coupled protons and Nuclear Overhauser Enhancements (NOEs) using the program NMRViewJ. The first step was to find resonances, which belonged to amino acids with distinguishable chemical shift ranges and coupling patterns, and low abundance in the sequence. NOEs arising from signals of two different amino acids were used to assign the amino acids sequentially, for detailed connectivities used, see Table 1.3. In general nearly all proton backbone resonances and many proton sidechain resonances could be assigned. Only a few <sup>13</sup>C and <sup>15</sup>N resonances could be assigned because of the poor spectral resolution of the highly abundant amino acids leucine and isoleucine.

Table 1.2: List of recorded 2D experiments using Sample 6

Experiment	Correlated Nuclei	Correlations Seen
TOCSY	$^1\text{H } ^1\text{H}$	crosspeaks of nuclei in an unbroken chain of couplings <sup>[46]</sup>
NOESY	$^1\text{H } ^1\text{H}$	crosspeaks of nuclei in close spatial proximity
$^{13}\text{C}$ -HSQC	$^{13}\text{C } ^1\text{H}$	peaks for protons attached to $^{13}\text{C}$
$^{15}\text{N}$ -HSQC	$^{15}\text{N } ^1\text{H}$	peaks for protons attached to $^{15}\text{N}$

Table 1.3: List of inter amino acid NOEs

Type	HN→HN	H <sub>α</sub> →HN	H <sub>α</sub> →H <sub>β</sub>
general	i→i+1	i→i+1	
α-Helix	i→i+2	i→i+3	i→i+3

### 1.2.4 Structure Calculation

The 3D structure calculation was done utilizing inter amino acid NOEs and TALOS angles. NOEs were calibrated using peak volumes and the mean peak volume was set to correspond to an empirical average distance.

TALOS angles were derived using TALOS-N (included in NMRPipe), which used the amino acid sequence and chemical shift assignments of HN, H<sub>α</sub>, C<sub>α</sub>, C<sub>β</sub>, CO and N to compare heptapeptide fragments of the peptide sequence with a database of high resolution structures.<sup>[50]</sup> The backbone torsion angles  $\phi$  and  $\psi$  of the best 25 matches were plotted in a Ramachandran-style plot and evaluated regarding the consistency of the result. Only strong predictions corresponding to all matches being within a standard deviation of 35° or less were used for the calculation.

The structure calculation was done using the Crystallography and NMR System (CNS).<sup>[51, 52]</sup> The first step was to generate a structure file of the amino acid sequence using the script *generate\_seq.inp*. The second script *generate\_extended.inp* generated an extended amino acid chain with optimized geometry. Using the script *anneal.inp* with the NOE and TALOS angle constraints with the extended amino acid chain as input, 100 structures were calculated.

The calculated structure of tm-ToxR in TFE (see Figure 1.5), represented by the 17 lowest energy structures with a rmsd of 0.435 and the backbone of amino acids 8-20 aligned, contains an α-helical part with a flexible part at the N-terminus. The significance of this result is discussable, since TFE does not resemble a procaryotic cellular membrane to the extent as micelles of surfactants like SDS and DPC do. α-helices are common in transmembrane domains, because every amino acid (except proline) has at least two polar groups: the amino group N-H and the carbonyl group C=O. These backbone groups tend to assemble α-helices to minimize contact with the hydrophobic environment of the cell membrane.

### 1.2.5 Unlabelled Protein Expression

Plasmid DNA of MBP-tm-ToxR and Z2-tm-ToxR isolated from *Escherichia coli* (*E. coli*) BL21 Star<sup>TM</sup> (DE3) One Shot<sup>®</sup> cells grown overnight in LB-Medium were sequenced with the dideoxynucleotide chain termination method<sup>[53]</sup> by services of LGC Genomics Berlin, Germany, to confirm the correct sequence of the constructs.

LB-Media (1 L) were inoculated (1:100) with overnight cultures of *E. coli* BL21 Star<sup>TM</sup> (DE3) One Shot<sup>®</sup> cells carrying pETMBP or pETZ2 respectively, induced with isopropyl β-D-thiogalactopyranosid (IPTG) (1 mM, OD<sub>600</sub> 0.6) and sampled at 0, 0.5, 1, 2, 3, 4, 5, 24 hours after induction to check for expression via Sodium dodecyl sulfate polyacrylamide gel electrophoresis (SDS-PAGE) (15 % acrylamide, 50 min, 200 V, see Figure 1.6 and 1.7). Both constructs showed overexpres-

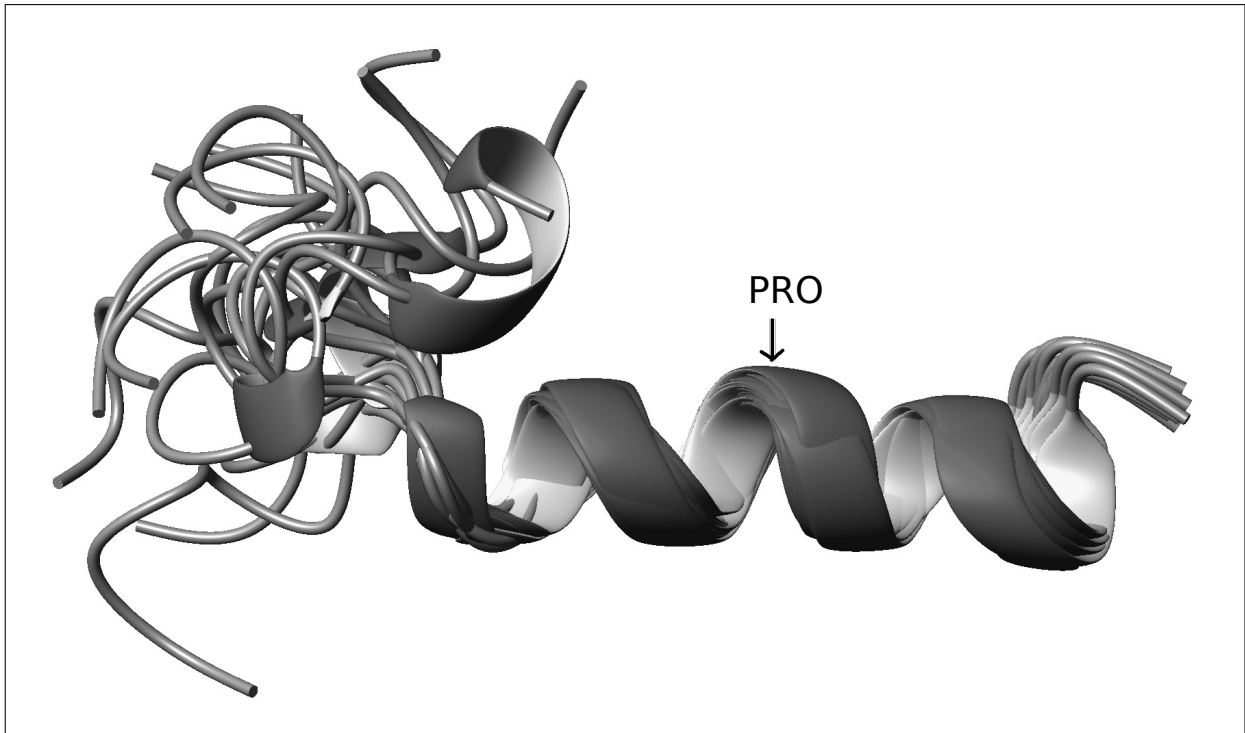


Figure 1.5: Calculated 3D structures of tm-ToxR, showing the 17 lowest energy structures with a rmsd of 0.435 and the backbone of amino acids 8-20 aligned

sion using the Prestained Protein Marker, Broad Range (7-175 kDa) from New England Biolabs® as a molecular weight standard and Coomassie staining. The properties of the constructs were calculated using ProtParam from the ExPASy Server.<sup>[54]</sup>

Protein for purification was grown in LB-media (1 L, 37 °C) after inoculation (1:100), induced with IPTG (1 mM, OD<sub>600</sub> 0.9) and grown at 20 °C over night.

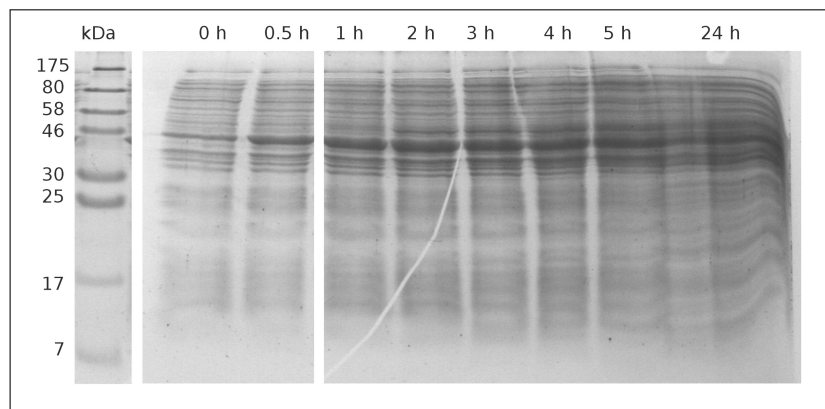


Figure 1.6: SDS-PAGE of MBP-tm-ToxR (~45 kDa) expression, sampled after induction

### 1.2.6 SDS Polyacrylamide Gel Electrophoresis

SDS-PAGE gels were prepared according to Table 1.4 containing the amounts for two gels. The stacking and the separating gel are prepared separately, and APS 10 % and TEMED have to be added last. The separating gel was prepared first and polymerized for 30 min with a thin layer of propanol on top. Then the propanol was removed and the prepared stacking gel was added on top

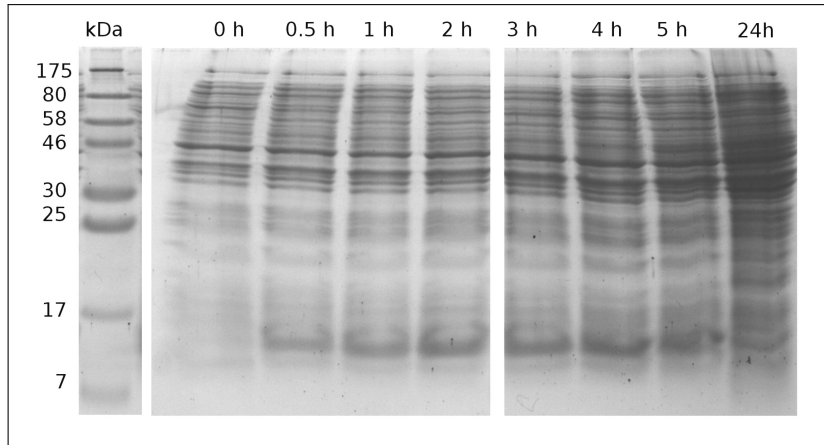


Figure 1.7: SDS-PAGE of Z2-tm-ToxR (~13 kDa) expression, sampled after induction

of the separating gel and polymerized for 30 min.

Table 1.4: Reagents for preparation SDS polyacrylamide gels

	Separating Gel		Stacking Gel
	12.5 %	15 %	
dH <sub>2</sub> O	4.175 mL	3.55 mL	2.92 mL
Polyacrylamide	3.125 mL	3.75 mL	0.5 mL
Separating Buffer	2.5 mL	2.5 mL	
Stacking Buffer			0.5 mL
APS 10 %	100 $\mu$ L	100 $\mu$ L	40 $\mu$ L
SDS 10 %	100 $\mu$ L	100 $\mu$ L	40 $\mu$ L
TEMED	5 $\mu$ L	5 $\mu$ L	4 $\mu$ L

### 1.2.7 Protein Purification

Cells were harvested (15 min, 5700 rpm, 4 °C), the pellet resuspended in Washing Buffer 1 (20 mL) and Protease Inhibitor Mix HP (100  $\mu$ L) from Serva, Heidelberg, Germany, sonicated on ice (15 min, Amplitude: 75 %, 0.55 s pulse, 0.55 s pause for native purification and 3 s pulse, 3 s pause for denaturing purification) and centrifuged (1 h, 13500 rpm, 4 °C).

The purification was done under native conditions, using Ni-NTA Agarose residue (~2 mL) in a 20 mL gravity flow column. At first the column was washed with distilled H<sub>2</sub>O (dH<sub>2</sub>O) (20 mL, 0.02 % NaN<sub>3</sub>) and equilibrated with Washing Buffer 1 (20 mL). The sterile filtered supernatant from the cell lysate was loaded onto the column, washed with Washing Buffer 1 (15 mL), Washing Buffer 2 (15 mL), Washing Buffer 3 (10 mL), Washing Buffer 4 (10 mL), eluted with Elution Buffer (10 mL) and the fractions collected on ice. The column was cleaned with Elution Buffer (20 mL), dH<sub>2</sub>O (20 mL, 0.02 % NaN<sub>3</sub>), Ethanol in dH<sub>2</sub>O (20 mL, 20 %), and filled with Ethanol in dH<sub>2</sub>O (20 %) for storage.

The result was analyzed using SDS-PAGE (12.5 % acrylamide, 40 min, 200 V, see Figure 1.8 and 1.9). MBP-tm-ToxR (~45 kDa) was isolated in the Elution Buffer fraction, with additional protein remaining in the insoluble fraction of the cell lysate, the protein concentration of the Elution Buffer fraction was determined using a NanoDrop 2000 to be 0.65 mg/mL and the properties of MBP-tm-ToxR calculated using ProtParam<sup>[54]</sup> (45.6 kDa,  $\epsilon_{280} = 67\,840$ ). Z2-tm-ToxR could not be purified because it did not bind to the column, but some might have been present in the insoluble protein fraction.

The supernatant of the insoluble protein fraction resuspended in urea (8 M) was used for purification under denaturing conditions following the same protocol as above, just preparing the Washing and Elution Buffers in urea (8 M) instead of dH<sub>2</sub>O. Additional MBP-tm-ToxR could be purified, which was refolded using Buffer 2, yielding a protein concentration of 0.36 mg/mL.

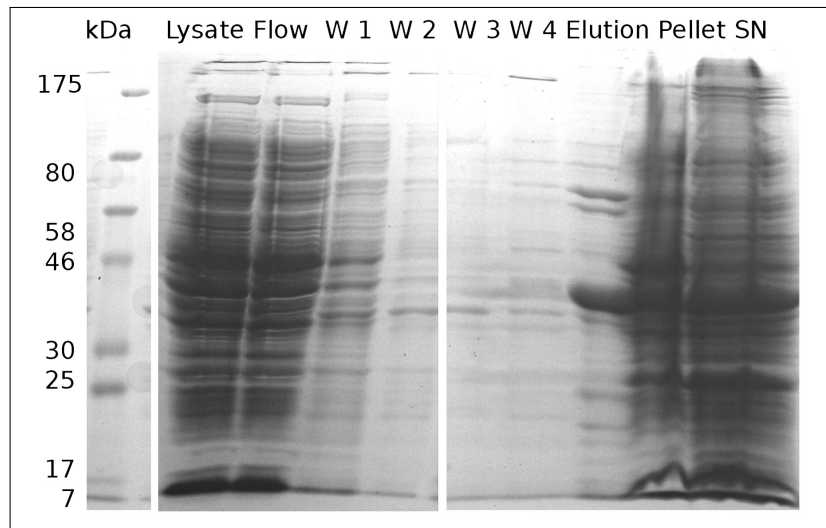


Figure 1.8: SDS-PAGE of purification of MBP-tm-ToxR under native conditions with the lanes containing: cell lysate, flow through, Washing Buffer 1, 2, 3, 4, Elution Buffer, insoluble pellet, supernatant of insoluble pellet resuspended in Urea (8 M)

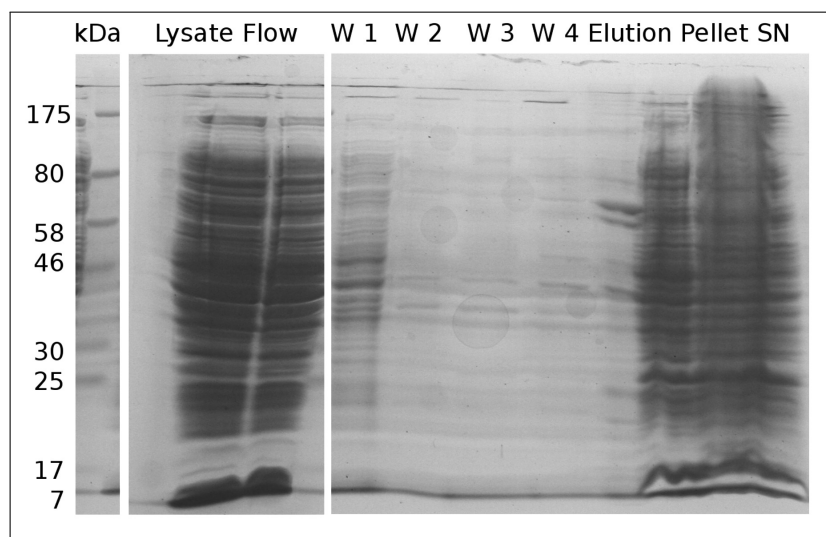


Figure 1.9: SDS-PAGE of purification of Z2-tm-ToxR under native conditions with the lanes containing: cell lysate, flow through, Washing Buffer 1, 2, 3, 4, Elution Buffer, insoluble pellet, supernatant of insoluble pellet resuspended in Urea (8 M)

### 1.2.8 TEV Cleavage

The protein was cleaved with Tobacco Etch Virus (TEV) protease (5 mL MBP-tm-ToxR in Elution Buffer, 2  $\mu$ L  $\beta$ -Mercaptoethanol, 1 mL TEV Protease solution), the mixture was shaken gently over night at room temperature. The difference between MBP and MBP-tm-ToxR could not be resolved with SDS-PAGE (15 % Acrylamide, 200 V) using the different time periods of 50 min and 135 min.

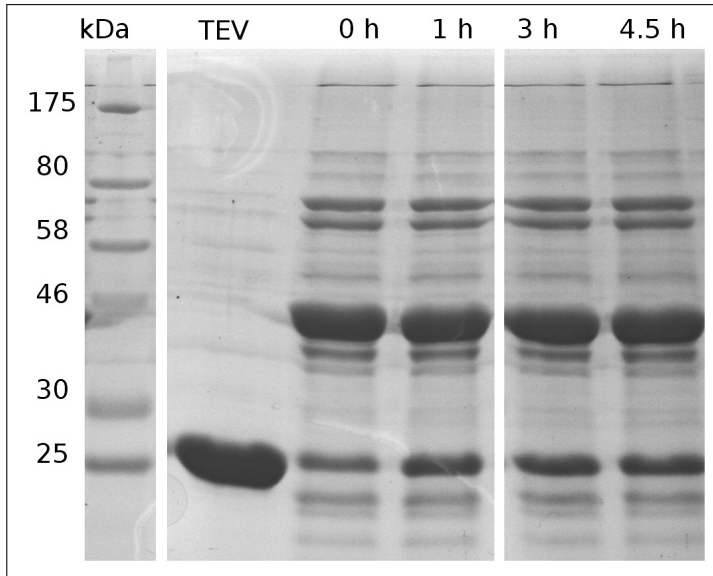


Figure 1.10: SDS-PAGE of TEV protease and time-points of the TEV cleavage of MBP-tm-ToxR

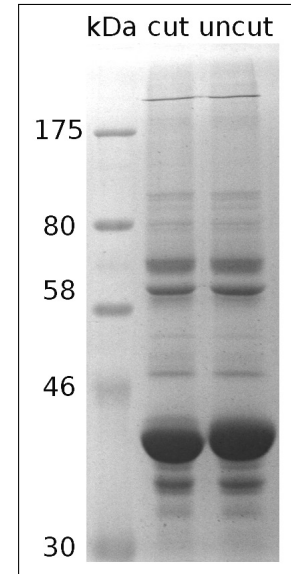


Figure 1.11: Overrun SDS-PAGE of overnight TEV cleavage

### 1.2.9 Mass Spectrometry

Two samples for Matrix Assisted Laser Desorption Ionization - Time of Flight (MALDI-TOF) Mass Spectrometry (MS) were prepared by washing MBP and MBP-tm-ToxR in 10 kDa cutoff Centricon-Tubes with Buffer 2 and concentrating them to final concentrations of 7 mg/mL and 18 mg/mL respectively.

Table 1.5: Overview of protein properties and MS results

Protein	MW	$\epsilon_{280}$	Concentration	MW determined by MS
MBP	43.2 kDa	67 840	7 mg/mL	42.9 kDa
MBP-tm-ToxR	45.6 kDa	67 840	18 mg/mL	43.7 kDa

The expression and purification of the construct MBP-tm-ToxR in pETMBP was readily achieved (see Figure 1.8), but at the applied conditions degradation was an issue. SDS-PAGE of the TEV cleavage starting material and product (see Figure 1.11) did not separate MBP and MBP-tm-ToxR, a difference of 2.4 kDa which should be observable. Furthermore, the results from MS indicated, that after purification the transmembrane domain was already shortened, because the TEV cleavage of the protein only shortened it by 0.8 kDa instead of the desired 2.4 kDa. The corresponding spectra can be viewed in Appendix 3.2.2. The accessibility of the TEV-cleavage site should have been sufficient.

### 1.2.10 Preparation of Samples for NMR Spectroscopy

MBP-tm-ToxR for NMR spectroscopy was prepared in  $^{15}\text{N}$ -labelled Minimal Medium (1L, 37 °C) after inoculation (1:50), induced with IPTG (1 mM, OD<sub>600</sub> 0.8) and grown at 25 °C over night. Gravity Flow Ni-NTA purification under native conditions was performed as described above, to yield 1.15 mg/mL protein. The protein was dialyzed (Buffer 3, over night) and purified further using a Sephadex<sup>®</sup>-75 prep grade Size Exclusion Chromatography (SEC) column with Buffer 3 (see Figure 1.12). SDS-PAGE was used to visualize the result (see Figure 1.13).

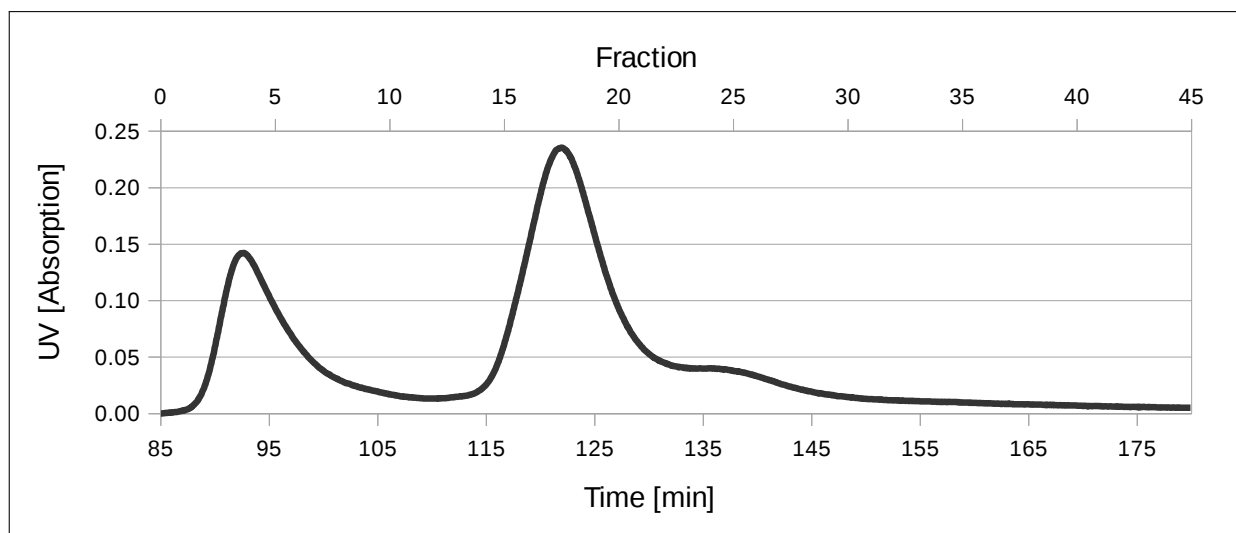


Figure 1.12: Chromatogram of the SEC

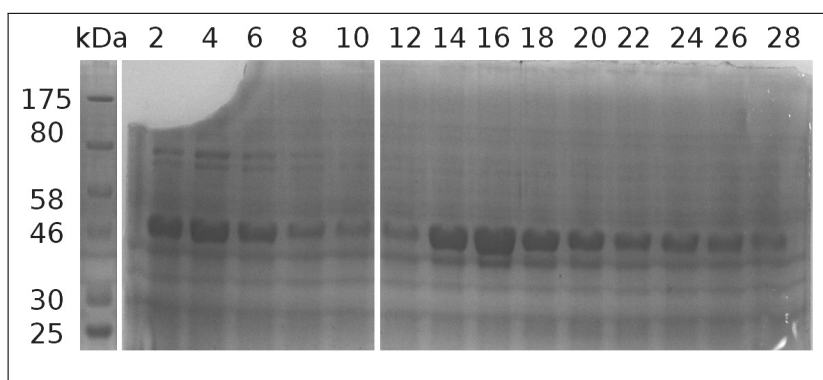


Figure 1.13: SDS-PAGE of SEC fractions

The combined fractions (14-21) from the column were dialyzed (Buffer 4, 2 days) and concentrated to record a  $^{15}\text{N}$ -HSQC spectrum of MBP-tm-ToxR in 90 % Buffer 4 and 10 %  $\text{D}_2\text{O}$ . The sample was diluted in Buffer 5 (10 mL) and n-dodecyl phosphocholine (DPC) (9.7 mg) and concentrated in a 3 kDa cutoff Centricon-Tube to a volume of 1 mL. TEV Protease solution (500  $\mu\text{L}$ ) and DPC (9.8 mg) were added to the concentrated protein and shaken gently over night. The cut protein was diluted with Buffer 5 (8.5 mL) and separated using a washed and equilibrated Gravity Flow Ni-NTA column. The flow-through (15 mL) was collected and the His<sub>6</sub>-tag bound protein eluted using Elution Buffer (10mL). The flow-through containing tm-ToxR and the Elution Buffer fraction containing MBP were dialyzed and concentrated with Buffer 4 in 3 kDa and 10 kDa cutoff Centricon-Tubes respectively.

SEC of  $^{15}\text{N}$ -labelled MBP-tm-ToxR showed that only minor impurities remain after the Ni-NTA gravity flow purification, but some aggregation was observed (see Figures 1.12 and 1.13).  $^{15}\text{N}$ -HSQC spectra of MBP and MBP-tm-ToxR show some differences (see Figure 1.14), which should correspond to the non-degraded part of tm-ToxR being cut off by the TEV protease.

### 1.2.11 NMR Spectroscopy

$^{15}\text{N}$ -HSQC spectra of both concentrated fractions in 90 % Buffer 4 and 10 %  $\text{D}_2\text{O}$  were recorded on a Bruker Avance III 700 MHz NMR spectrometer equipped with a Triple-Resonance CryoProbe at 300 K.



After the TEV cleavage some signals were expected to disappear, but the stacked spectra of MBP and MBP-tm-ToxR show only some shifted signals. This does not account for the loss of a 2.4 kDa peptide at its C-terminus.

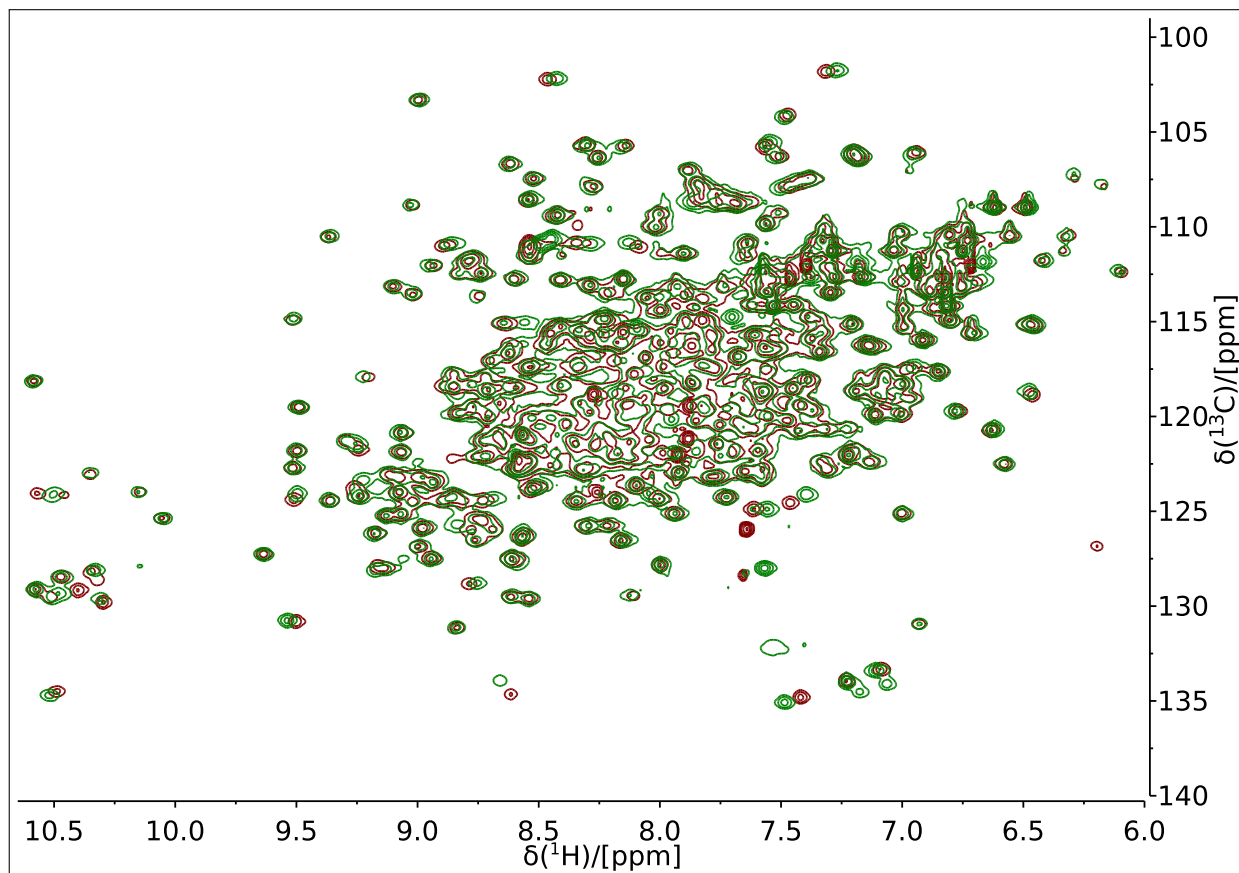


Figure 1.14: Stacked  $^{15}\text{N}$ -HSQC spectra of MBP (red) and MBP-tm-ToxR (green)

### 1.3 Discussion

The involvement of the tm-ToxR in a regulatory function of ToxR remains unsolved. The calculated structure indicates a possibility of the  $\alpha$ -helix to be prone to structural rearrangement, because of the proline residue, which is known to be an  $\alpha$ -helix breaker. Such changes could be triggered by homodimerization or by heterodimerization with ToxS.

Environmental factors influencing the transcription regulation of genes and structures of proteins in *V. cholerae*: bile being important for TcpP dimerization facilitating its activity<sup>[28]</sup> and interacting with OmpU and OmpT,<sup>[30, 31]</sup> cholesterol and unsaturated fatty acids enhancing the motility of *V. cholerae*,<sup>[33]</sup> anaerobiosis activating AphB, the interaction between ToxR and TcpP and the expression of colonization factors in the El Tor strain,<sup>[37-40]</sup> bicarbonate enhancing and oleic acid inhibiting the activity of ToxT<sup>[34, 35]</sup> and the phosphate regulation associated protein PhoB repressing the transcription of *tcpPH*.<sup>[17]</sup>

A novel dependence is postulated, the tolerance of ToxR regulated OmpU to bile is required for TcpP homodimerization.

The recombinant expression of tm-ToxR is thought to not have worked correctly due to incomplete translation or fast degradation of the tm-ToxR part of the construct. For future expressions a lower incubation temperature after the induction has been suggested.

## 2 Improvements to the Slice-Selective Instant Homonuclear Decoupling

### 2.1 Introduction

Pure shift pulse sequences to record Nuclear Magnetic Resonance (NMR) spectra with suppressed proton homonuclear couplings have become a state of the art technique to enhance resolution in NMR spectroscopy. Several techniques have been established with different applications and drawbacks: slice-selective instant homonuclear decoupling,<sup>[55, 56]</sup> bilinear rotation decoupling (BIRD)<sup>[57–59]</sup> and pure shift yielded by chirp excitation (PSYCHE).<sup>[60]</sup> Introducing varied data chunk durations and shifted frequency pulses to instant slice-selective decoupling has further improved this method.<sup>[61]</sup>

#### 2.1.1 Slice-Selective Instant Homonuclear Broadband Decoupling

The original slice-selective decoupling pulse sequence (see Figure 2.1) utilizes soft  $90^\circ$  radiofrequency (RF) pulses during a weak magnetic field gradient for exciting different proton resonances in each slice, called the active spins. This is followed by the decoupling block consisting of a hard and a soft  $180^\circ$  RF pulse during a weak magnetic field gradient between a pair of  $\tau_{inc}/2$ . This block only refocuses the couplings associated with the active spins, but coupling between two active spins, also called strong coupling is not refocused.  $\tau_{inc}$  is incremented starting at 0. During processing the first part of each increment's time domain (a data chunk, see Equation 2.1) is used to reconstruct one fully decoupled free induction decay (FID).<sup>[55]</sup>

$$\text{data chunk length} = \frac{\text{number of increments}}{\text{size of time domain}} \quad (2.1)$$

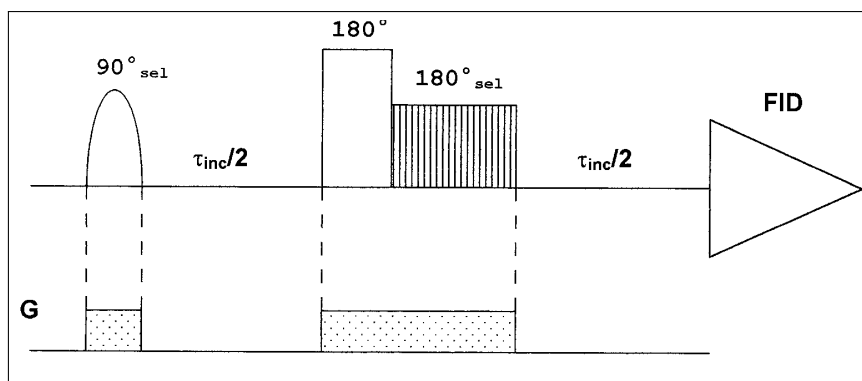


Figure 2.1: The Slice-Selective Decoupling Pulse Sequence (figure taken from<sup>[55]</sup>)

Improving the original slice-selective decoupling scheme to record a full FID in one scan, has greatly increased its viability. This is achieved by periodically pausing data acquisition for a short duration and applying the decoupling block (see Figure 2.2). Additionally homonuclear couplings are now refocused in the middle of one acquisition block instead of refocusing it at the beginning of acquisition to enable faster acquisition. Purging gradients enclosing both  $180^\circ$  RF pulses have been added as well.<sup>[56]</sup>

The sensitivity of this type of experiment is the major drawback, because of the slice selective excitation the sensitivity decreases to a few percent of a non-decoupled spectrum. The chemical shift difference of coupled spins that can be decoupled depends on the width of the selective 180° RF pulse.

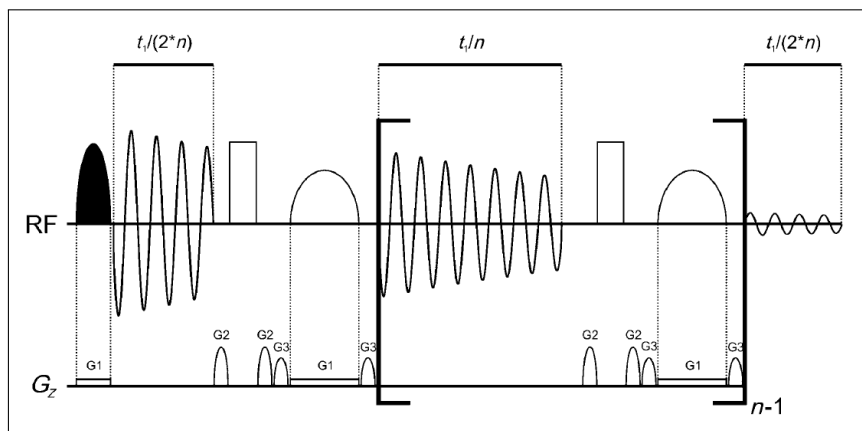


Figure 2.2: The Slice-Selective Instant Homonuclear Broadband Decoupling Pulse Sequence (figure taken from<sup>[56]</sup>)

### 2.1.2 Bilinear Rotational Decoupling

BIRD utilizes the heteronuclear coupling between <sup>1</sup>H (I spin) and <sup>13</sup>C (S spin) to differentiate between protons bound to <sup>12</sup>C and <sup>13</sup>C. This is achieved by employing the BIRD element (see Figure 2.3). The element starts with the excitation of all proton resonances with a hard 90°<sub>y</sub> RF pulse followed by a spin echo with an evolution time of 1/2J<sub>CH</sub> and 180°<sub>x</sub> RF pulses to <sup>1</sup>H and <sup>13</sup>C. After the first evolution time, spins coupled to <sup>13</sup>C are aligned with the y-axis and therefore their net magnetization is not affected by the 180° RF pulses. The final hard 90°<sub>y</sub> RF pulse transfers the spins coupled to <sup>13</sup>C to the +z axis and all other spins to the -z axis.<sup>[57]</sup>

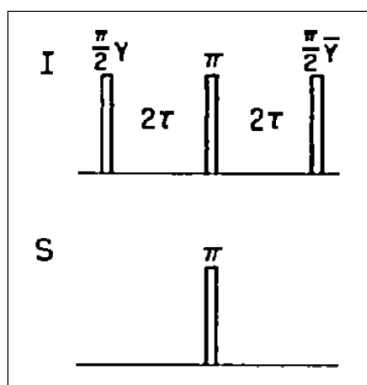


Figure 2.3: The basic BIRD element (figure taken from<sup>[57]</sup>)

The modern BIRD sequence (see Figure 2.4) starts by exciting all proton resonances using a hard 90° pulse (narrow rectangle), after  $\tau_1$  proton resonances experience a hard 180° pulse (wide rectangle) and <sup>13</sup>C resonances experience a 180° broadband inversion pulse (BIP)<sup>[62]</sup> (dotted wide rectangle with a diagonal line), which is only applied every second scan, to subtract signals from protons bound to <sup>12</sup>C, enabling access to protons only bound to <sup>13</sup>C. The BIRD element is used to refocus heteronuclear couplings at the beginning of acquisition and homonuclear coupling in the middle of the data chunk. Additionally <sup>13</sup>C broadband decoupling is turned on during acquisition.

By incrementation of  $t_1$  and using the first part of each FID to construct fully decoupled FIDs a fully decoupled spectrum can be recorded.<sup>[58]</sup>

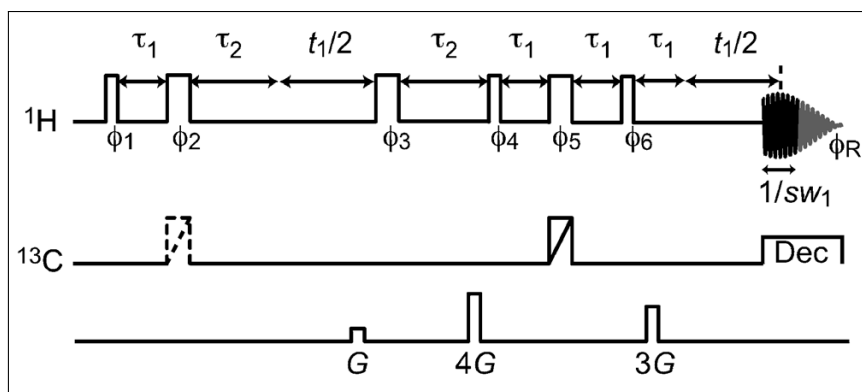


Figure 2.4: The BIRD Pulse Sequence (figure taken from<sup>[58]</sup>)

The sensitivity of this experiment is limited to the natural abundance of  $^{13}\text{C}$ , which is 1.1 %. By employing this technique in HSQC spectra which are already limited to the natural abundance of the heteronucleus, no further loss of sensitivity occurs<sup>[63]</sup>.

This method has also been improved to be able to acquire an FID in a single scan. This is achieved by using trains of BIRD-based homonuclear decoupling in combination with initial INEPT-based filtering of  $^{13}\text{C}$ -bound protons.<sup>[59]</sup>

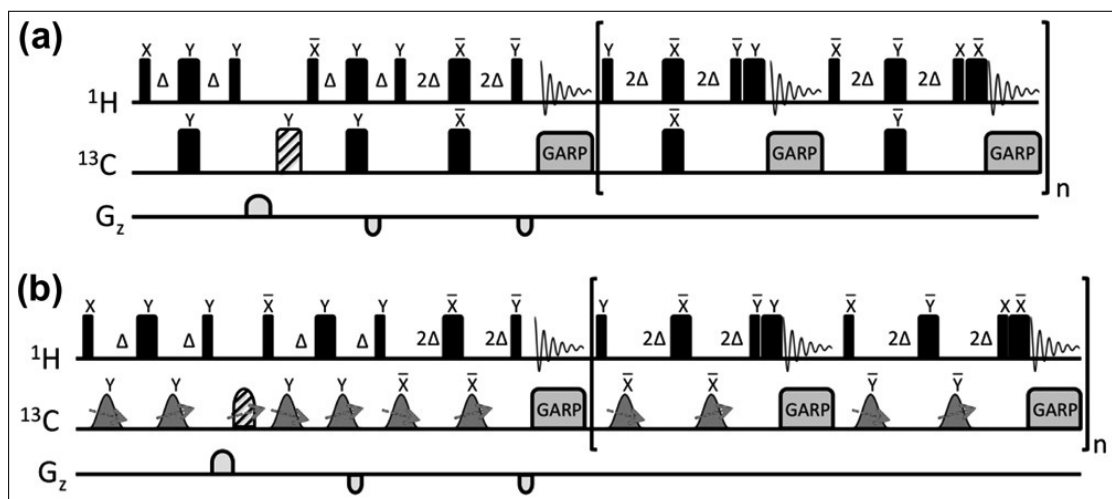


Figure 2.5: The BIRD Pulse Sequence for instant homonuclear broadband decoupling with (a)  $^{13}\text{C}$  hard pulses (b)  $^{13}\text{C}$  broadband frequency-swept pulses (figure taken from<sup>[59]</sup>)

### 2.1.3 PSYCHE

In the beginning all resonances are excited with a hard  $90^\circ$  pulse (thin filled rectangle), after  $t_1/2$  time all spins are inverted using a hard  $180^\circ$  pulse (broad filled rectangle), flanked by purging gradients  $G_1$ . Then two low flip angle swept-frequency pulses during a weak gradient field (trapeze with arrows), flanked by purging gradients are employed. After another  $t_1/2$  a FID chunk is recorded for  $t_2$ . Incrementation of  $t_1$  enables access to a whole FID, which is reconstructed from the recorded chunks.

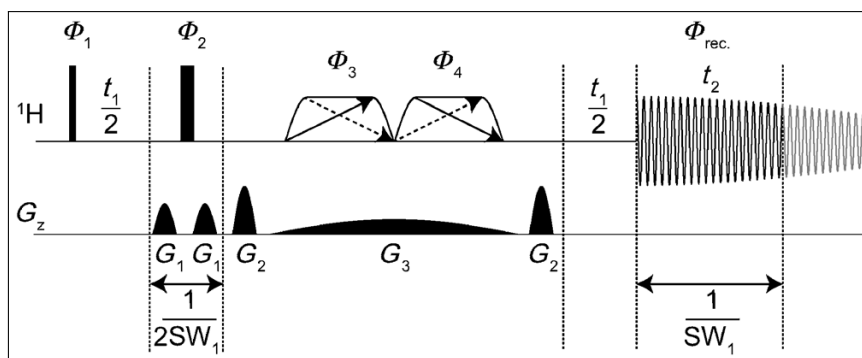


Figure 2.6: The PSYCHE Pulse Sequence (figure taken from<sup>[60]</sup>)

## 2.2 Methods

### 2.2.1 Artifact Suppression by using a Variable Data Chunk Lengths

Using data chunks to record NMR data gives rise to artifacts that occur on both sides of real NMR signals. They originate from scalar coupling evolution during the acquisition of the data chunks. The artifacts arise symmetrically at frequencies proportional to the reciprocal value of the data chunk duration. Variation of the data chunk durations shifts the frequencies of the artifact peaks (see Figure 2.7). Varying this durations  $n$  times lowers their intensities to about  $1/n$ , enabling even the  $^{13}\text{C}$ -satellites to be distinguished from the artifacts (see Figure 2.8). This is achieved by defining an optimized data chunk length and multiplying it with a factor that is varied throughout the experiment (see Appendix 3.2.5).

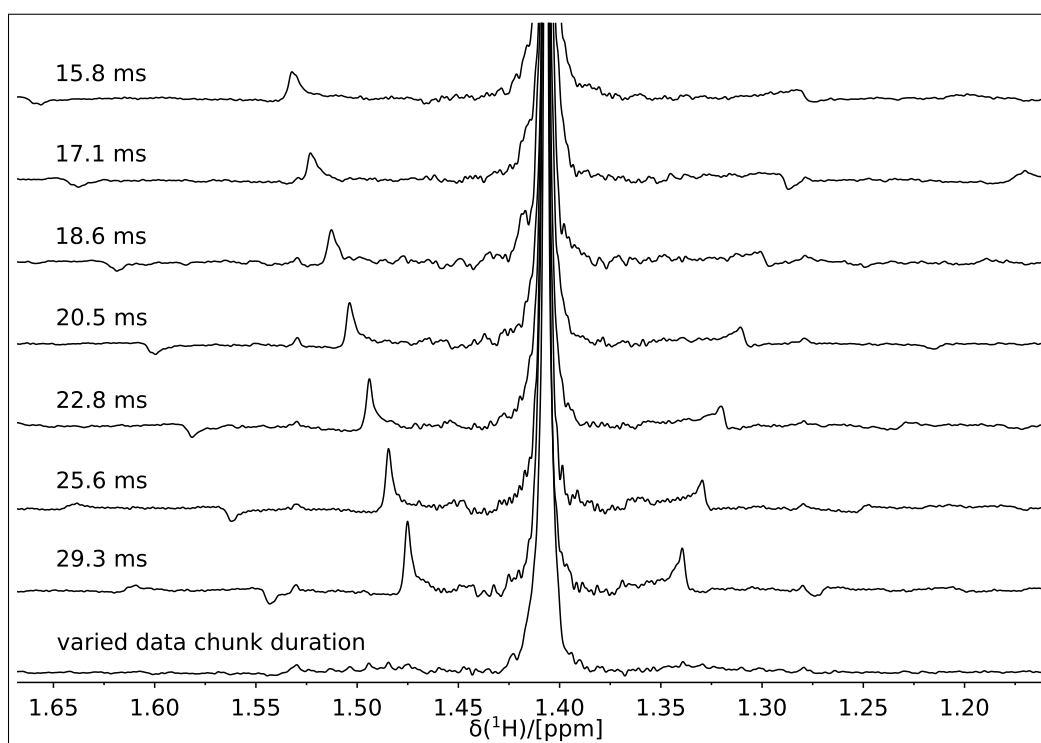


Figure 2.7: Enlarged stacked spectra of  $n$ -propanol (10 %,  $d_6$ -DMSO, 256 scans), showing the shifting of the decoupling sidebands with different data chunk lengths and a spectrum varying these seven data chunk durations

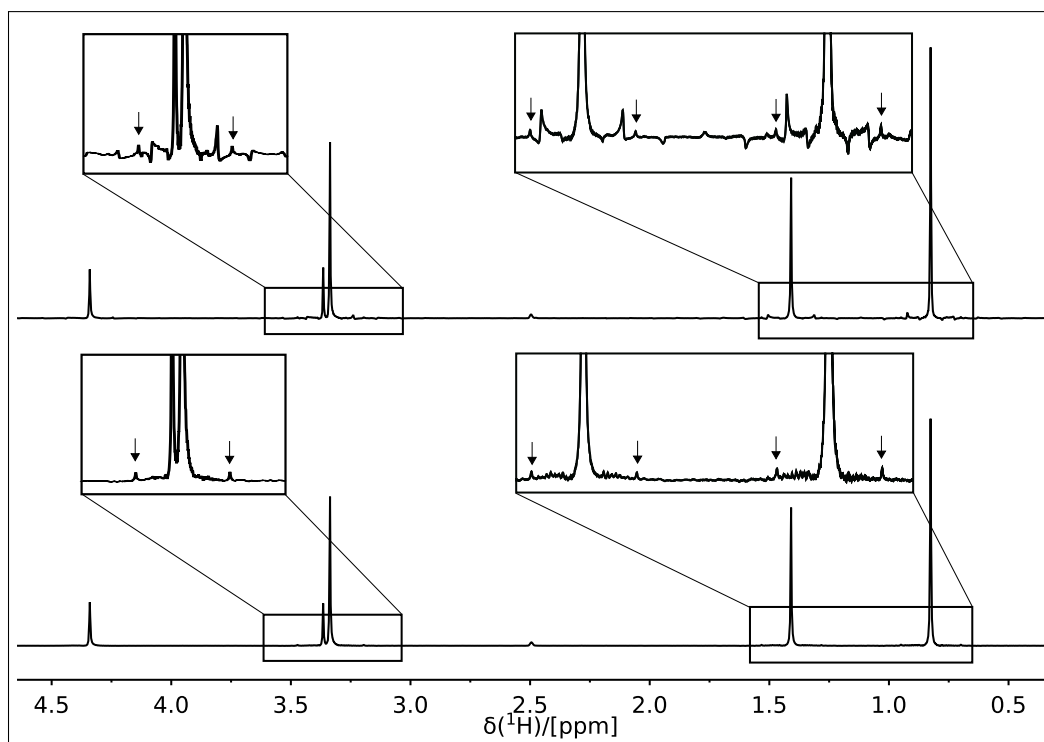


Figure 2.8: Comparing two spectra of *n*-propanol (10 %,  $d_6$ -DMSO, 8192 scans) with (bottom) and without (top) the use of varied data chunk lengths, and arrows indicating  $^{13}\text{C}$ -satellites in the enlarged regions

## 2.2.2 Shorter Acquisition Times by Relaxation Delay Reduction using Frequency Shifted Pulses

Employing frequency shifted pulses in spatially selective experiments to access unused magnetization and enable faster pulsing has already been used to enhance the classic slice-selective decoupling method.<sup>[64]</sup> It has also been used for the faster acquisition of regular non-decoupled 1D spectra.<sup>[65]</sup>

For sufficient independently manipulable magnetization to be accessible by the frequency shifted selective  $90^\circ$  and  $180^\circ$  pulses, the weak magnetic field gradient has to be doubled. This leads to a loss of about half of the signal intensity, which is usually overcome by the higher signal intensity and the ability to record scans faster by using frequency shifted pulses.

This method employs eight frequency offsets for the frequency shifted pulses (see Appendix 3.2.4 for the correspondent shapelists), they are ordered systematically to contain big gaps between the consecutive offsets. The input of the frequency shifts is done using shape lists containing the power level of the pulse in dB, the offset alignment, the frequency shift in Hz and the name of the pulse shape. The frequency shift input has to be a multiple of  $\pm 100$  Hz otherwise problems have been encountered. The offset alignment defines the timepoint during the pulse experiencing the precise flip angle, with 0 being the beginning of the pulse and 1 being the end of the pulse.

The effect of frequency shifted pulses was visualized using *n*-propanol and 3,4-dimethoxyphenyl)-ethylamine (DMPEA) (see Figures 2.9, 2.10, 2.11 and 2.12). There are three main effects, the increase in signal intensity per second per proton, the shifting of the interscan delay length value yielding the highest signal per second per proton and the more uniform signal response over all protons, which is most pronounced for the aromatic protons of DMPEA (see Figure 2.12).

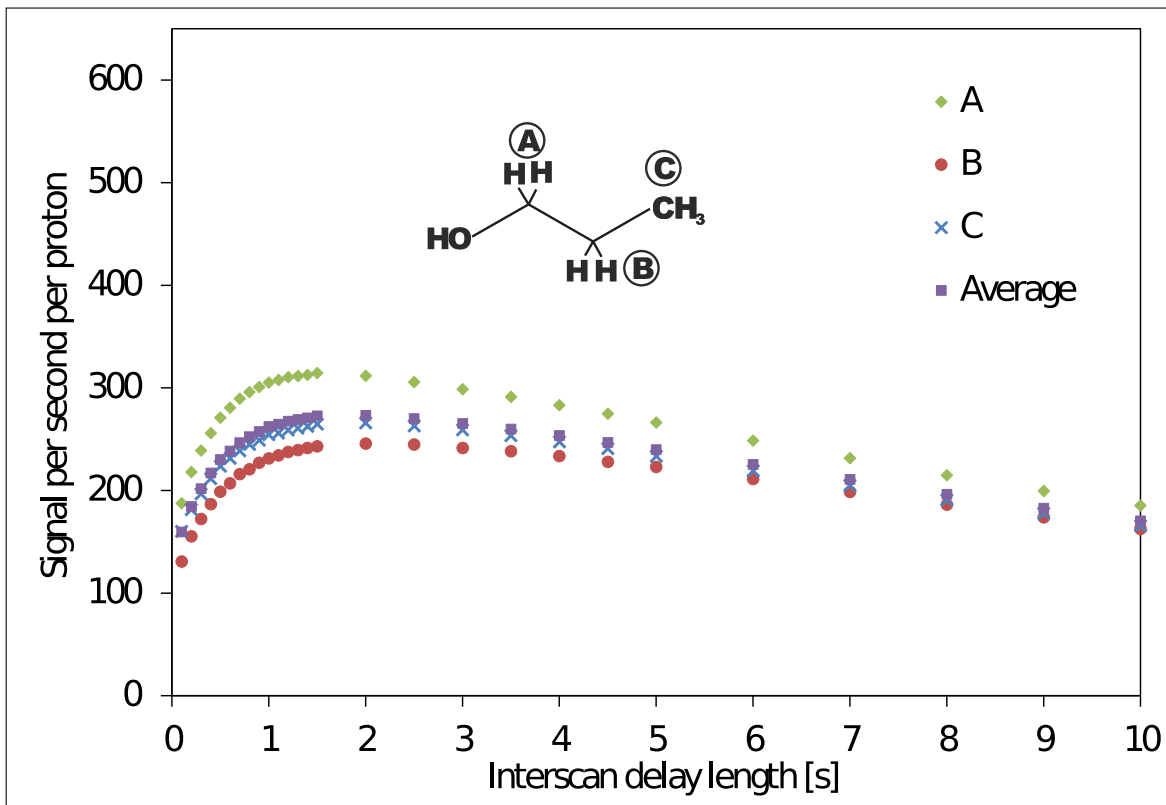


Figure 2.9: Signal intensities per proton per second of measurement time for different protons of *n*-propanol at different interscan delay lengths without using frequency shifted pulses

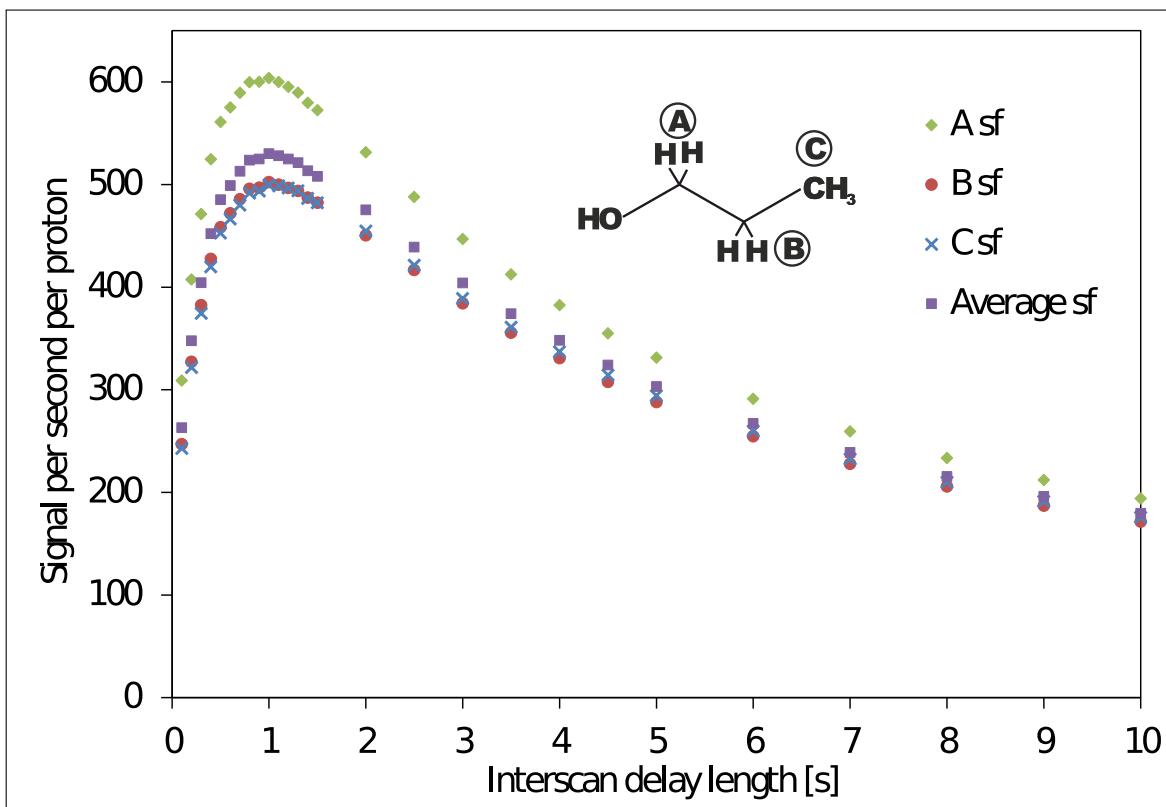


Figure 2.10: Signal intensities per proton per second of measurement time for different protons of *n*-propanol at different interscan delay lengths when using frequency shifted pulses

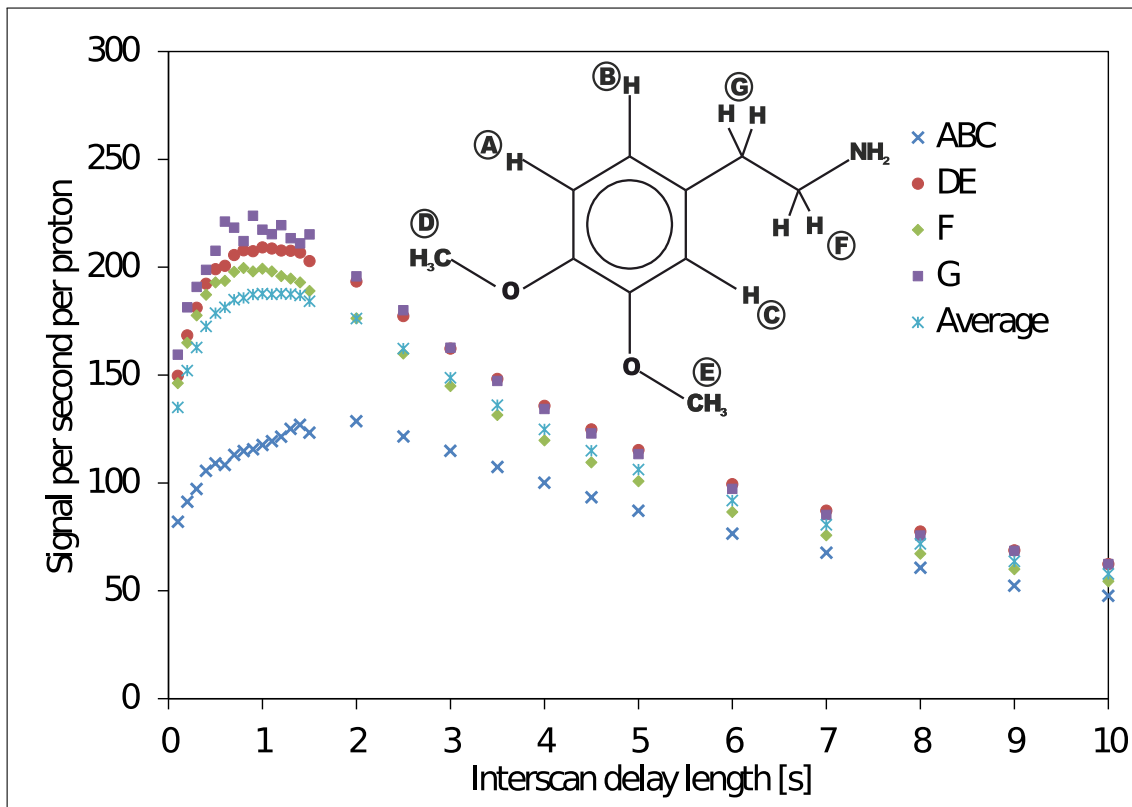


Figure 2.11: Signal intensities per proton per second of measurement time for different protons of DMPEA at different interscan delay lengths without using frequency shifted pulses

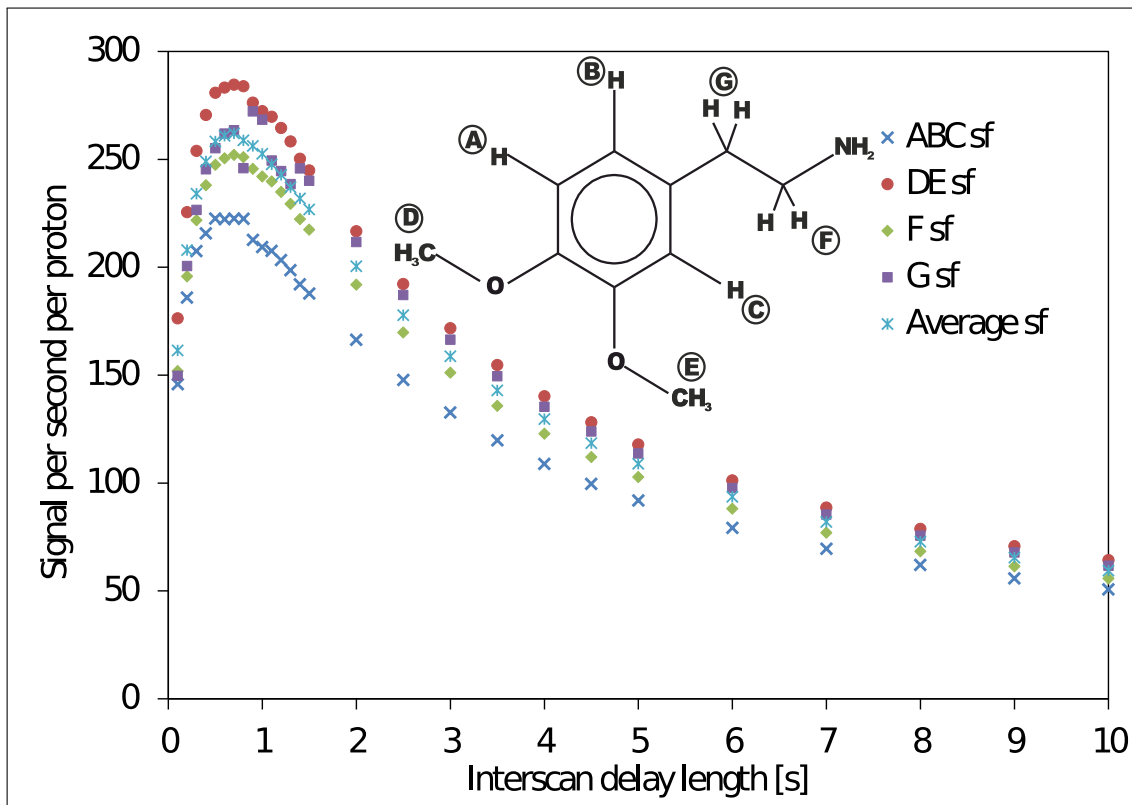


Figure 2.12: Signal intensities per proton per second of measurement time for different protons of DMPEA at different interscan delay lengths when using frequency shifted pulses



## 2.3 Discussion

Using variable data chunk lengths enables the use of slice-selective decoupling experiments for compound mixtures with an extended concentration range, because the suppression of artifacts prevents mistaking artifacts for signals of compounds with a lower concentration and vice versa. The range of factors to be used is limited, because greater data chunk lengths increase the intensity of the artifacts due to longer scalar coupling evolution during the data chunk acquisition and shorter data chunk lengths reduce the overall signal intensity due to longitudinal relaxation.

There are some drawbacks in using frequency shifted pulses, the weak magnetic field gradient has to be doubled, which leads to a loss of 50 % signal intensity. This is overcome by the increase in signal intensity and the ability to perform more scans per measurement time by using frequency shifted pulses. Additionally, signals from slices close to the edge of the sensitive volume experience a non-linear gradient, signal distortions caused by this effect are mitigated by using frequency shifted pulses. Application of both concepts at the same time works well.

## 3 Appendix

### 3.1 Materials

#### 3.1.1 Bacterial Strains, Enzymes, Kits and Plasmids

<i>E. coli</i> BL21 Star <sup>TM</sup> (DE3) One Shot <sup>®</sup>	Life Technologies, Carlsbad, USA
TEV protease	Umeå University, Sweden
peqGOLD Plasmid DNA Miniprep Kit II	Peqlab GmbH, Erlangen, Germany

Table 3.1: List of used EMBL expression vectors from Umeå University, Sweden

Plasmid	Construct	Description
pETMBP	MBP-tm-ToxR	Kan <sup>R</sup> , expresses His <sub>6</sub> -tag, Maltose Binding Protein (MBP), TEV-cleavage site, tm-ToxR
pETZ2	Z2-tm-ToxR	Kan <sup>R</sup> , expresses His <sub>6</sub> -tag, IgG binding domain (Z-domain) of <i>Staphylococcus aureus</i> protein A (Z2), TEV-cleavage site, tm-ToxR

#### 3.1.2 Media and Stocks

<b>Minimal Medium <sup>15</sup>N-labelled (1L)</b>	<b>Micro salts (1.000x stock)</b>
6.8 g Na <sub>2</sub> HPO <sub>4</sub>	1.5 M ZnCl <sub>2</sub>
3.0 g KH <sub>2</sub> PO <sub>4</sub>	150 mM CaCl <sub>2</sub>
0.5 g NaCl	50 mM H <sub>3</sub> BO <sub>3</sub>
3.0 g Glucose	20 mM FeCl <sub>3</sub>
0.7 g <sup>15</sup> NH <sub>4</sub> Cl	800 μM CuCl <sub>2</sub>
1 mL micro salts (1.000x stock)	150 μM CoCl <sub>2</sub>
1 mL MgSO <sub>4</sub> (1.000x stock)	15 μM (NH <sub>4</sub> ) <sub>6</sub> Mo <sub>7</sub> O <sub>24</sub> x 4 H <sub>2</sub> O
1 mL Kanamycin (1.000x stock)	
<b>LB-Medium (1L)</b>	<b>Kanamycin (1.000x stock)</b>
20 g LB-Broth	50 mg/mL Kanamycin
1 mL Kanamycin (1.000x stock)	
<b>MgSO<sub>4</sub> (1.000x stock)</b>	<b>IPTG (1.000x stock)</b>
1 M MgSO <sub>4</sub>	1 M IPTG

### 3.1.3 Buffers

For denaturing purification Washing Buffers 1-4 and Elution Buffer were prepared in Urea (8 M) instead of water.

Table 3.2: List of prepared and used buffers, with 0.02 %  $\text{NaN}_3$  added

Washing Buffer 1 (25 mL)	Washing Buffer 2 (25 mL)	Washing Buffer 3 (25 mL)
40 mM Tris	40 mM Tris	40 mM Tris
20 mM Imidazol	20 mM Imidazol	20 mM Imidazol
60 mM NaCl	60 mM NaCl	400 mM NaCl
4 mM $\beta$ -Mercaptoethanol pH 8.0	4 mM $\beta$ -Mercaptoethanol pH 8.0	4 mM $\beta$ -Mercaptoethanol pH 8.0
Washing Buffer 4 (25 mL)	Elution Buffer (25 mL)	Buffer 1
40 mM Tris	40 mM Tris	50 mM $\text{KH}_2\text{PO}_4$
40 mM Imidazol	660 mM Imidazol	pH 5.0
60 mM NaCl	60 mM NaCl	
4 mM $\beta$ -Mercaptoethanol pH 8.0	4 mM $\beta$ -Mercaptoethanol pH 8.0	
Buffer 2	Buffer 3	Buffer 4
25 mM Tris pH 7.5	50 mM Tris 300 mM NaCl pH 8.0	50 mM Tris 50 mM NaCl pH 6.5
Buffer 5	Buffer 6	Buffer 7
50 mM Tris 300 mM NaCl 2 mM $\beta$ -Mercaptoethanol 1 mM EDTA pH 8.0		

Table 3.3: List of buffers used for SDS-PAGE

Separating Buffer	Stacking Buffer	Running Buffer (10x stock)
1.5 M TrisHCl pH 8.8	1 M TrisHCl pH 6.8	3.03 g/L TrisHCl 14.4 g/L Glycine 1 g/L SDS
Coomassie Staining	Coomassie Destaining	
450 mL Methanol	450 mL Methanol	
450 distilled $\text{H}_2\text{O}$	450 distilled $\text{H}_2\text{O}$	
100 mL Acetic acid	100 mL Acetic acid	
2.5 g Coomassie		

### 3.2 Data

#### 3.2.1 Sequences

Table 3.4: Sequence of ToxR

MFGLG	HNSKE	ISMSH	IGTKF	ILAEK	FTFDP	LSNTL	IDKED	SEEII	RLGSN	ESRIL	WLLAQ
RPNEV	ISRND	LHDFV	WREQG	FEVDD	SSLTQ	AISTL	RKMLK	DSTKS	PQYVK	TVPKR	GYQLI
ARVET	VEEEM	ARESE	AAHDI	SQPES	VNEYA	ESSSV	PSSAT	VVNTF	QPANV	VTNKS	APNLG
NRLLI	LIAVL	LPLAV	LLLTN	PSQTS	FKPLT	VVDGV	AVNMP	NNHPD	LSNWL	PSIEL	CVKKY
NEKHT	GGLKP	IEVIA	TGGQN	NQLTL	NYIHS	PEVSG	ENITL	RIVAN	PNDAL	KVCE	

Table 3.5: Sequences of used Peptides

synthetic tm-ToxR	NLG	NRLLI	LIAVL	LPLAV	LLLTN
recombinant tm-ToxR	G	NRLLI	LIAVL	LPLAV	LLLTN PS

#### 3.2.2 Mass Spectroscopy Spectra

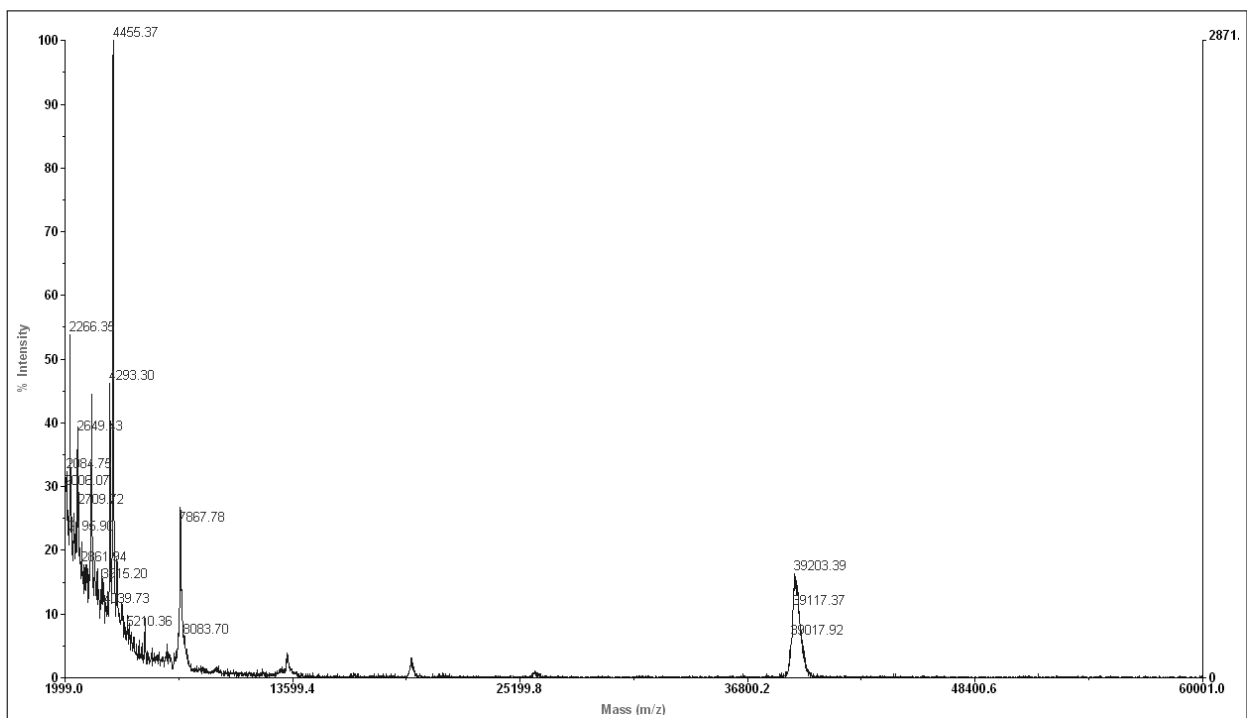


Figure 3.1: MALDI-TOF reference spectrum of Aldolase from rabbit muscle

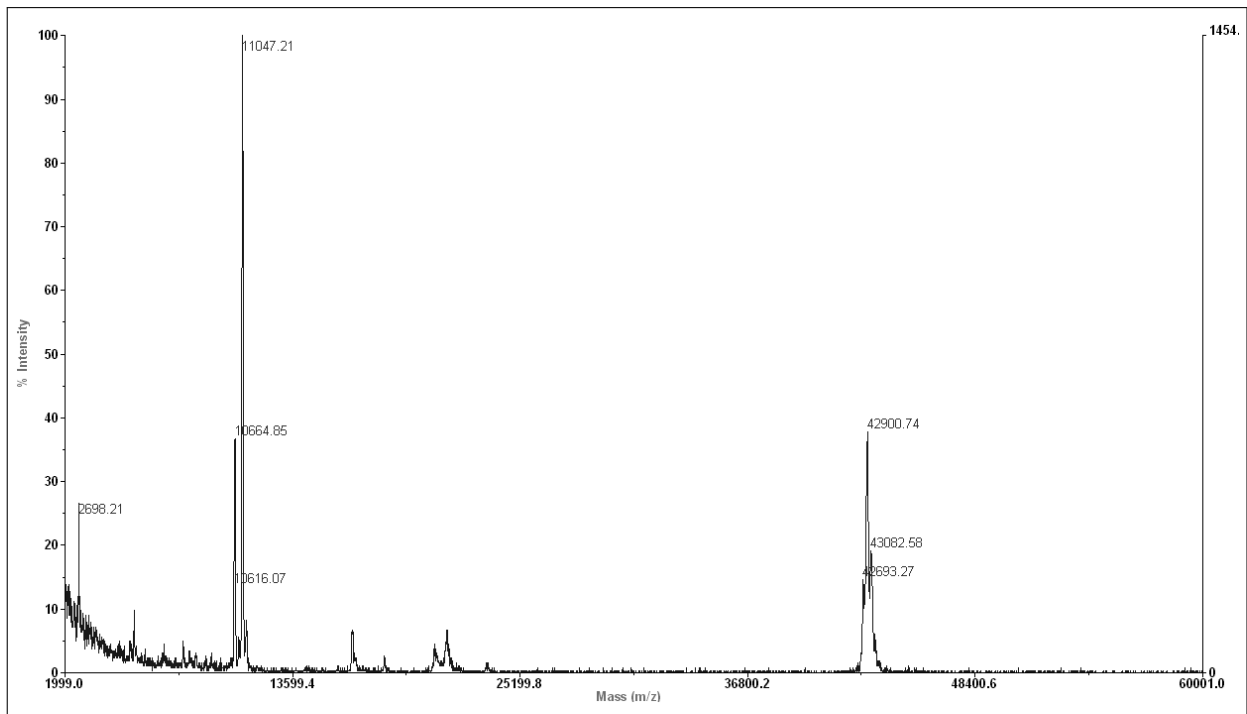


Figure 3.2: MALDI-TOF spectrum of MBP

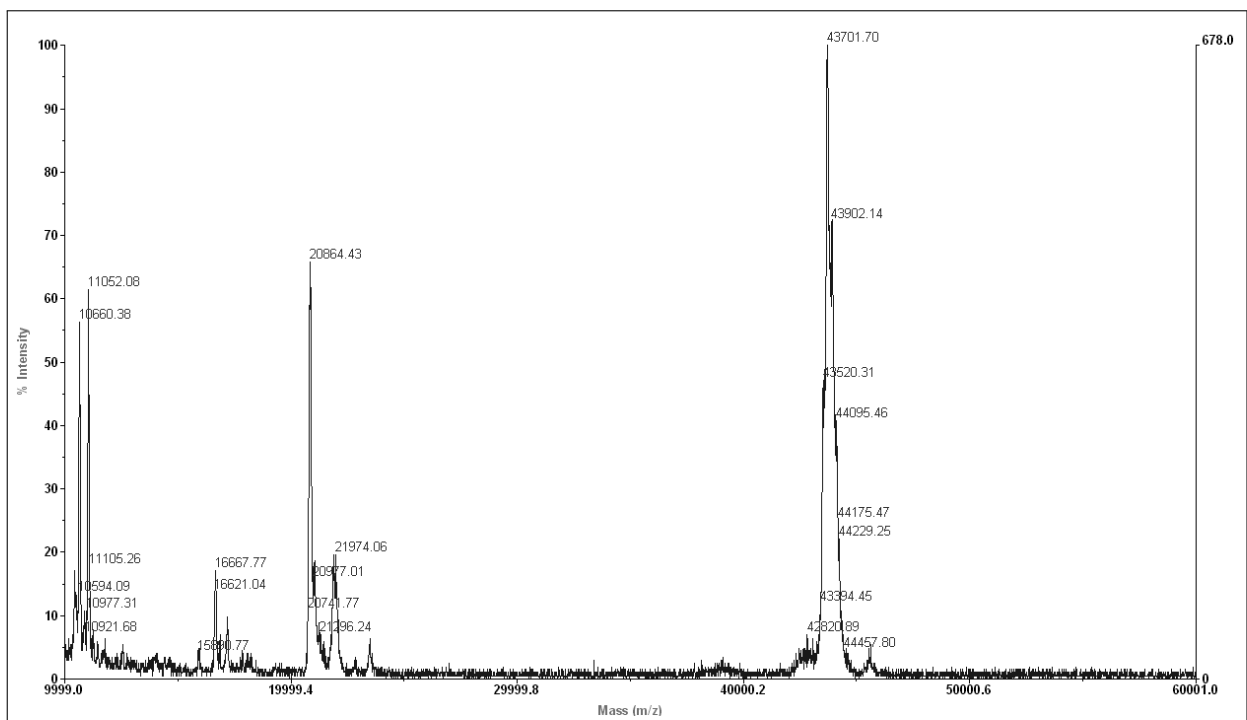


Figure 3.3: MALDI-TOF spectrum of MBP-tm-ToxR

### 3.2.3 Pulse Sequences

```
;zgadc2
;avance-version (06/01/20)
;1D sequence with explicit programming of acquisition
;
;$CLASS=HighRes
;$DIM=1D
;$TYPE=
;$SUBTYPE=
;$COMMENT=

#include <Avance.incl>
#include <De.incl>
#include <Grad.incl>
#include <Delay.incl>

define list<shape> SPL_90 = <spl_90_jm21>
define list<shape> SPL_180 = <spl_180_jm21>
define list<delay> Dlist = <$VDLIST>

dwellmode explicit

"d11=3u"
"d12=6.5u"
"d20=10u"
"l2=10*20"
"l1=l2-1"
"d2=aq/l2"
"d3=d2/2"
"p2=2*p1"

1 ze
2 3m

#ifdef VLC
  "l5=l2*Dlist"
  "l1=l5-1"
  "d2=aq/l5"
  "d3=d2/2"
#endif

4u BLKGRAD
d1 rpp2
50u UNBLKGRAD

d12 p10:f1
d12 gron1
#ifdef SF
  (p12:SPL_90 ph1)
#endif
```

```
#ifndef SF
    (p12:sp12 ph1)
#endif
d12 groff
d12 pl1:f1

ACQ_START(ph30,ph31)

    0.05u DWL_CLK_ON
    0.1u REC_UNBLK
d3:r
    0.1u REC_BLK
    0.05u DWL_CLK_OFF

p16:gp2
d16 pl1:f1
p2 ph2
p16:gp2
d16

p16:gp3
d16 pl0:f1
10u
d11 gron1
#endif SF
    (p13:SPL_180 ph3)
#endif
#ifndef SF
    (p13:sp13 ph3)
#endif
d11 groff
10u
p16:gp3
d16

3 0.05u DWL_CLK_ON
    0.1u REC_UNBLK
d2:r
    0.1u REC_BLK
    0.05u DWL_CLK_OFF

p16:gp2
d16 pl1:f1
p2 ph2
p16:gp2
d16

p16:gp3
d16 pl0:f1
10u
d11 gron1
```

```
#ifdef SF
    (p13:SPL_180 ph3)
#endif
#ifndef SF
    (p13:sp13 ph3)
#endif
    d11 groff
    10u
    p16:gp3
    d16

lo to 3 times l1

    0.05u DWL_CLK_ON
    0.1u REC_UNBLK
    d3
    25m
    0.1u REC_BLK
    0.05u DWL_CLK_OFF

#ifdef SF
    10u SPL_90.inc
    10u SPL_180.inc
#endif
#ifdef VLC
    10u Dlist.inc
#endif

rcyc=2

wr #0

exit

ph1 = 0 2 2 0 1 3 3 1
ph2 = 0 2
ph3 = 2 0
ph30= 0
ph31= 0 2 2 0 1 3 3 1

;p11 : f1 channel - power level for pulse (default)
;p1 : f1 channel - high power pulse
;d1 : relaxation delay; 1-5 * T1
;NS: 1 * n, total number of scans: NS * TD0
;l0: input loopcounter, good d2 range: 20-25ms
;l5: varied loopcounter, redefined during aquisition
;gpz1: 1 %, 2 % for -DSF
;gpz2: 11 %
;gpz3: 5 %

;$Id: zgadc,v 1.12 2009/07/02 16:40:47 ber Exp $
```



### 3.2.4 Shape Lists

#### spl\_90\_jm21

```
#Power[dB] Offset[Hz] Offset alignment Shape file name
42.69 dB 1200 0.5 Eburp2.1000
42.69 dB -800 0.5 Eburp2.1000
42.69 dB 400 0.5 Eburp2.1000
42.69 dB 1600 0.5 Eburp2.1000
42.69 dB -1600 0.5 Eburp2.1000
42.69 dB -400 0.5 Eburp2.1000
42.69 dB 800 0.5 Eburp2.1000
42.69 dB -1200 0.5 Eburp2.1000
```

#### spl\_180\_jm21

```
#Power[dB] Offset[Hz] Offset alignment Shape file name
37.68 dB 1200 0.5 Gaus1_180r.1000
37.68 dB -800 0.5 Gaus1_180r.1000
37.68 dB 400 0.5 Gaus1_180r.1000
37.68 dB 1600 0.5 Gaus1_180r.1000
37.68 dB -1600 0.5 Gaus1_180r.1000
37.68 dB -400 0.5 Gaus1_180r.1000
37.68 dB 800 0.5 Gaus1_180r.1000
37.68 dB -1200 0.5 Gaus1_180r.1000
```

### 3.2.5 Delay List

```
0.7
0.725
0.75
0.775
0.8
0.825
0.85
0.875
0.9
0.925
0.95
0.975
1.0
1.025
1.05
1.075
1.1
1.125
1.15
1.175
1.2
1.225
1.25
1.275
1.3
```

### 3.3 List of Acronyms

<i>E. coli</i>	<i>Escherichia coli</i>
BIP	broadband inversion pulse
BIRD	bilinear rotation decoupling
cFP	cyclo(Phe-Pro)
CNS	Crystallography and NMR System
CT	cholera toxin
d <sub>2</sub> -TFE	deuterated 2,2,2-Trifluoro ethanol
dH <sub>2</sub> O	distilled H <sub>2</sub> O
DMPEA	3,4-dimethoxyphenyl)-ethylamine
DPC	n-dodecyl phosphocholine
FID	free induction decay
H-NS	histone-like nucleoid structuring protein
HSQC	Heteronuclear Single Quantum Correlation
IPTG	isopropyl $\beta$ -D-thiogalactopyranosid
MALDI-TOF	Matrix Assisted Laser Desorption Ionization - Time of Flight
MBP	Maltose Binding Protein
MS	Mass Spectrometry
NMR	Nuclear Magnetic Resonance
NOE	Nuclear Overhauser Enhancement
NOESY	Nuclear Overhauser Enhancement Spectroscopy
omp	outer membrane porin
PSYCHE	pure shift yielded by chirp excitation
RF	radiofrequency
SDS-PAGE	sodium dodecyl sulfate polyacrylamide gel electrophoresis
SEC	Size Exclusion Chromatography
TCP	toxin-coregulated pilus
TEV	Tobacco Etch Virus
tm-ToxR	transmembrane domain of ToxR
TOCSY	Total Correlation Spectroscopy
wHTH	winged Helix Turn Helix DNA binding motif
Z2	IgG binding domain (Z-domain) of <i>Staphylococcus aureus</i> protein A

### 3.4 References

- [1] S. M. Faruque, M. J. Albert, and J. J. Mekalanos. Epidemiology, Genetics, and Ecology of Toxigenic *Vibrio cholerae*. *Microbiol. Mol. Biol. Rev.* **1998**, *62*, 1301–1314. DOI: 10.1111/j.1348-0421.2002.tb02659.x.
- [2] J. Reidl and K. E. Klose. *Vibrio cholerae* and cholera: out of the water and into the host. *FEMS Microbiol. Rev.* **2002**, *26*, 125–139. DOI: 10.1016/S0168-6445(02)00091-8.
- [3] F. H. Yildiz and K. L. Visick. *Vibrio* biofilms: so much the same yet so different. *Trends Microbiol.* **2009**, *17*, 109–118. DOI: 10.1016/j.tim.2008.12.004.
- [4] S. J. Krebs and R. K. Taylor. Protection and Attachment of *Vibrio cholerae* Mediated by the Toxin-Coregulated Pilus in the Infant Mouse Model. *J. Bacteriol.* **2011**, *193*, 5260–5270. DOI: 10.1128/JB.00378-11.
- [5] D. Vanden Broeck, C. Horvath, and M. J. S. De Wolf. *Vibrio cholerae*: Cholera toxin. *Int. J. Biochem. Cell Biol.* **2007**, *39*, 1771–1775. DOI: 10.1016/j.biocel.2007.07.005.

- [6] J. S. Matson, J. H. Withey, and V. J. DiRita. Regulatory Networks Controlling *Vibrio cholerae* Virulence Gene Expression. *Infect. Immun.* **2007**, *75*, 5542–5549. DOI: 10.1128/IAI.01094-07.
- [7] S. Kanjilal, R. Citorik, R. C. LaRocque, M. F. Ramoni, and S. B. Calderwood. A Systems Biology Approach To Modeling *Vibrio cholerae* Gene Expression under Virulence-Inducing Conditions. *J. Bacteriol.* **2010**, *192*, 4300–4310.
- [8] M. B. Nye, J. D. Pfau, K. Skorpupski, and R. K. Tylor. *Vibrio cholerae* H-NS Silences Virulence Gene Expression at Multiple Steps in the ToxR Regulatory Cascade. *J. Bacteriol.* **2000**, *182*, 4295–4303.
- [9] A. Ghosh, K. Paul, and R. Chowdhury. Role of the Histone-Like Nucleoid Structuring Protein in Colonization, Motility, and Bile-Dependent Repression of Virulence Gene Expression in *Vibrio cholerae*. *Infect. Immun.* **2006**, *74*, 3060–3064. DOI: 10.1128/IAI.74.5.3060-3064.2006.
- [10] C. C. Häse and J. J. Mekalanos. TcpP protein is a positive regulator of virulence gene expression in *Vibrio cholerae*. *Proc. Natl. Acad. Sci.* **1998**, *95*, 730–734.
- [11] D. E. Higgins and V. J. DiRita. Transcriptional control of *toxT*, a regulatory gene in the ToxR regulon of *Vibrio cholerae*. *Mol. Microbiol.* **1994**, *14*, 17–29. DOI: 10.1111/j.1365-2958.1994.tb01263.x.
- [12] E. S. Krukonis, R. R. Yu, and V. J. DiRita. The *Vibrio cholerae* ToxR/TcpP/ToxT virulence cascade: distinct roles for two membrane-localized transcription activator on a single promoter. *Mol. Microbiol.* **2000**, *38*, 67–84. DOI: 10.1046/j.1365-2958.2000.02111.x.
- [13] Y. Minato, S. R. Fassio, A. J. Wolfe, and C. C. Häse. Central metabolism controls transcription of a virulence gene regulator in *Vibrio cholerae*. *Microbiology* **2013**, *159*, 792–802. DOI: 10.1099/mic.0.064865-0.
- [14] G. Kovacikova and K. Skorupski. A *Vibrio cholerae* LysR Homolog, AphB, Cooperates with AphA at the *tcpPH* Promoter To Activate Expression of the ToxR Virulence Cascade. *J. Bacteriol.* **1999**, *181*, 4250–4256.
- [15] K. Skorupski and R. K. Taylor. A new level in the *Vibrio cholerae* ToxR virulence cascade: AphA is required for transcriptional activation of the *tcpPH* operon. *Mol. Microbiol.* **1999**, *31*, 763–771. DOI: 10.1046/j.1365-2958.1999.01215.x.
- [16] G. Kovacikova, W. Lin, and K. Skorupski. *Vibrio cholerae* AphA uses a novel mechanism for virulence gene activation that involves interaction with the LysR-type regulator AphB at the *tcpPH* promoter. *Mol. Microbiol.* **2004**, *53*, 129–142. DOI: 10.1111/j.1365-2958.2004.04121.x.
- [17] J. T. Pratt, A. M. Ismail, and A. Camilli. PhoB regulates both environmental and virulence gene expression in *Vibrio cholerae*. *Mol. Microbiol.* **2010**, *77*, 1595–1605. DOI: 10.1111/j.1365-2958.2010.07310.x.
- [18] X. Xu, A. M. Stern, Z. Liu, B. Kan, and J. Zhu. Virulence regulator AphB enhances *toxR* transcription in *Vibrio cholerae*. *BMC Microbiol.* **2010**, *10*. DOI: 10.1186/1471-2180-10-3.
- [19] G. Kovacikova and K. Skorupski. Regulation of virulence gene expression in *Vibrio cholerae* by quorum sensing: HapR functions at the *aphA* promoter. *Mol. Microbiol.* **2002**, *46*, 1135–1147. DOI: 10.1046/j.1365-2958.2002.03229.x.
- [20] W. Lin, G. Kovacikova, and K. Skorupski. The quorum sensing regulator HapR downregulates the expression of the virulence gene transcription factor AphA in *Vibrio cholerae* by antagonizing Lrp- and VpsR-mediated activation. *Mol. Microbiol.* **2007**, *64*, 953–967. DOI: 10.1111/j.1365-2958.2007.05693.x.

- [21] R. A. Finkelstein, M. Boesman-Finkelstein, Y. Chang, and C. C. Häse. Vibrio cholerae Hemagglutinin/Protease, Colonial Variation, Virulence, and Detachment. *Infect. Immun.* **1992**, *60*, 472–478.
- [22] A. T. Nielsen, N. A. Dolganov, G. Otto, M. C. Miller, C. Y. Wu, and G. K. Schoolnik. RpoS Controls the Vibrio cholerae Mucosal Escape Response. *PLoS Pathog.* **2006**, *2*, e109. DOI: 10.1371/journal.ppat.0020109.
- [23] X. R. Bina, D. L. Taylor, A. Virkam, V. M. Ante, and J. E. Bina. Vibrio cholerae ToxR Downregulates Virulence Factor Production in Response to Cyclo(Phe-Pro). *American Society* **2013**, *4*, e00366–13.
- [24] S. Chatterjee, M. Asakura, N. Chowdhury, S. B. Neogi, N. Sugimoto, S. Haldar, S. P. Awasthi, A. Hinenoya, S. Aoki, and Y. S. Capsaicin, a potential inhibitor of cholera toxin production in Vibrio cholerae. *FEMS Microbiol. Lett.* **2010**, *306*. DOI: 10.1111/j.1574-6968.2010.01931.x.
- [25] S. Yamasaki, M. Asakura, S. B. Neogi, A. Hinenoya, E. Iwaoka, and S. Aoki. Inhibition of virulence potential of Vibrio cholerae by natural compounds. *Indian J. Med. Res.* **2011**, *133*, 232–239.
- [26] T. J. Goss, S. J. Morgan, E. L. French, and E. S. Krukoni. ToxR Recognizes a Direct Repeat Element in the toxT, ompU, ompT, and ctxA Promoters of Vibrio cholerae To Regulate Transcription. *Infect. Immun.* **2013**, *81*, 884–895. DOI: 10.1128/IAI.00889-12.
- [27] V. H. I. Fengler, E. C. Boritsch, S. Tutz, A. Seper, H. Ebner, S. Roier, S. Schild, and J. Reidl. Disulfide Bond Formation and ToxR Activity in Vibrio cholerae. *PLoS One* **2012**, *7*. DOI: 10.1371/journal.pone.0047756.
- [28] M. Yang, Z. Liu, C. Hughes, A. M. Stern, H. Wang, Z. Zhong, B. Kan, W. Fenical, and J. Zhu. Bile salt-induced intermolecular disulfide bond formation activates Vibrio Cholera virulence. *Proc. Natl. Acad. Sci.* **2013**, *110*, 2348–2353. DOI: 10.1073/pnas.1218039110.
- [29] N. A. Beck, E. S. Krukoni, and V. J. DiRita. TcpH Influences Virulence Gene Expression in Vibrio cholerae by Inhibiting Degradation of the Transcription Activator TcpP. *J. Bacteriol.* **2004**, *186*, 8309–8316. DOI: 10.1128/JB.186.24.8309-8316.2004.
- [30] J. A. Wibbenmeyer, D. Provenzano, C. F. Landry, K. E. Klose, and A. H. Delcour. Vibrio cholerae OmpU and OmpT Porins Are Differentially Affected by Bile. *Infect. Immun.* **2002**, *70*, 121–126. DOI: 10.1128/IAI.70.1.121-126.2002.
- [31] D. Provenzano and K. E. Klose. Altered expression of the ToxR-regulated porins OmpU and OmpT diminishes Vibrio cholerae bile resistance, virulence factor expression, and intestinal colonization. *PNAS* **2000**, *97*, 10220–10224. DOI: 10.1073/pnas.170219997.
- [32] D. T. Hung and J. J. Mekalanos. Bile acids induce cholera toxin expression in Vibrio cholerae in a ToxT-independent manner. *Proc. Natl. Acad. Sci.* **2005**, *102*, 3028–3033. DOI: 10.1073/pnas.0409559102.
- [33] A. Chatterjee, P. K. Dutta, and C. R. Effect of Fatty Acids and Cholesterol Present in Bile on Expression of Virulence Factors and Motility of Vibrio cholerae. *Infect. Immun.* **2007**, *75*, 1946–1953. DOI: 10.1128/IAI.01435-06.
- [34] M. J. Lowden, K. Skorupski, M. Pellegrini, M. G. Chiorazzo, R. K. Taylor, and F. J. Kull. Structure of Vibrio cholerae ToxT reveals a mechanism for fatty acid regulation of virulence genes. *Proc. Natl. Acad. Sci.* **2010**, *107*, 2860–2865. DOI: 10.1073/pnas.0915021107.
- [35] B. H. Abuaita and J. H. Withey. Bicarbonate Induces Vibrio cholerae Virulence Gene Expression by Enhancing ToxT Activity. *Infect. Immun.* **2009**, *77*, 4111–4120. DOI: 10.1128/IAI.00409-09.

- [36] J. L. Taylor, R. S. De Silva, G. Kovacicova, W. Lin, R. K. Taylor, K. Skorupski, and F. J. Kull. The crystal structure of AphB, a virulence gene activator from *Vibrio cholerae*, reveals residues that influence its response to oxygen and pH. *Mol. Microbiol.* **2012**, *83*, 457–470. DOI: 10.1111/j.1365-2958.2011.07919.x.
- [37] Z. Liu, M. Yang, G. L. Peterfreund, A. M. Tsou, N. Selamoglu, F. Daldal, Z. Zhong, B. Kan, and J. Zhu. *Vibrio cholerae* anaerobic induction of virulence gene expression is controlled by thiol-based switches of virulence regulator AphB. *Proc. Natl. Acad. Sci.* **2011**, *108*, 810–815. DOI: 10.1073/pnas.1014640108.
- [38] G. Kovacicova, W. Lin, and K. Skorupski. The LysR-Type Virulence Activator AphB Regulates the Expression of Genes in *Vibrio cholerae* in Response to Low pH and Anaerobiosis. *J. Bacteriol.* **2010**, *192*, 4181–4191. DOI: 10.1128/JB.00193-10.
- [39] K. Marrero, A. Sánchez, A. Rodríguez-Ulloa, L. J. González, L. Castellanos-Serra, d. Paz-Lago, J. Campos, B. L. Rodríguez, E. Suzarte, L. t., G. Padrón, and R. Fando. Anaerobic growth promotes synthesis of colonization factors encoded at the *Vibrio* pathogenicity island in *Vibrio cholerae* El Tor. *Res. Microbiol.* **2009**, *160*, 48–56. DOI: 10.1016/j.resmic.2008.10.005.
- [40] F. Fan, Z. Liu, N. Jabeen, L. D. Birdwell, J. Zhu, and B. Kan. Enhanced Interaction of *Vibrio cholerae* Virulence Regulators TcpP and ToxR under Oxygen-Limiting Conditions. *Infect. Immun.* **2014**, *82*, 1676–1682. DOI: 10.1128/IAI.01377-13..
- [41] T. Chatterjee, R. P. Saha, and P. Chakrabarti. Structural studies on *Vibrio cholerae* ToxR periplasmic and cytoplasmic domains. *Biochim. Biophys. Acta* **2007**, *1774*, 1331–1338. DOI: 10.1016/j.bbapap.2007.08.003.
- [42] N. K. Gubensäk. Studying *Vibrio Cholerae* virulence regulators ToxR and ToxS by NMR spectroscopy. MA thesis. Karl-Franzens-Universität Graz, 2014.
- [43] E. M. Schrank. Investigation of Bacterial Regulatory Mechanisms by Solution NMR Spectroscopy. PhD thesis. Karl-Franzens-Universität Graz, 2014.
- [44] KEGG - Sequences of toxR. 13.08.2014. [http://www.genome.jp/dbget-bin/www\\_bget?ko:K10921](http://www.genome.jp/dbget-bin/www_bget?ko:K10921).
- [45] K. Hofmann and W. Stoffel. TMbase – a database of membrane spanning proteins segments. *Biol. Chem. Hoppe-Seyler* **1993**, *374*, 166.
- [46] J. Keeler. Understanding NMR Spectroscopy. John Wiley & Sons, Ltd, 2010.
- [47] F. Delaglio, S. Grzesiek, G. W. Vuister, G. Zhu, J. Pfeifer, and A. Bax. NMRPipe: a multidimensional spectral processing system based on UNIX pipes. *J. Biomol. NMR* **1995**, *6*, 277–293. DOI: 10.1007/BF00197809.
- [48] Biological Magnetic Resonance Data Bank - Statistics Calculated for All Chemical Shifts from Atoms in the 20 Common Amino Acids. 25.07.2014. [http://www.bmrwisc.edu/ref\\_info/statful.htm](http://www.bmrwisc.edu/ref_info/statful.htm).
- [49] A. Bundi and K. Wüthrich. <sup>1</sup>H-NMR Parameters of the Common Amino Acid Residues Measured in Aqueous Solutions of the Linear Tetrapeptides H-Gly-Gly-X-L-Ala-OH. *Biopolymers* **1979**, *18*, 285–297. DOI: 10.1002/bip.1979.360180206.
- [50] Y. Shen and A. Bax. Protein backbone and sidechain torsion angles predicted from NMR chemical shifts using artificial neural networks. *J. Biomol. NMR* **2013**, *56*, 227–241. DOI: 10.1007/s10858-013-9741-y.

- [51] A. T. Brünger, P. D. Adams, G. M. Clore, W. L. DeLano, P. Gros, R. W. Grosse-Kunstleve, J.-S. Jiang, J. Kuszewski, M. Nilges, N. S. Pannu, R. J. Read, L. M. Rice, T. Simonson, and G. L. Warren. Crystallography & NMR System: A New Software Suite for Macromolecular Structure Determination. *Acta Crystallogr.* **1998**, *D54*, 905–921. DOI: 10.1107/S0907444498003254.
- [52] A. T. Bruenger. Version 1.2 of the Crystallography and NMR system. *Nature Protocols* **2007**, *2*, 2728–2733. DOI: 10.1038/nprot.2007.406.
- [53] F. Sanger, S. Nicklen, and A. R. Coulson. DNA sequencing with chain-terminating inhibitors. *Proc. Natl. Acad. Sci.* **1977**, *74*, 5463–5467.
- [54] E. Gasteiger, H. C., A. Gattiker, S. Duvaud, M. R. Wilkins, R. D. Appel, and A. Bairoch. Protein Identification and Analysis Tools on the ExPASy Server. Ed. by J. M. Walker: The Proteomics Protocols Handbook. Humana Press, 2005, 571–607.
- [55] K. Zangger and H. Sterk. Homonuclear Broadband-Decoupled NMR Spectra. *J. Magn. Reson.* **1997**, *124*, 486–489. DOI: 10.1006/jmre.1996.1063.
- [56] N. H. Meyer and K. Zangger. Simplifying Proton NMR Spectra by Instant Homonuclear Broadband Decoupling. *Angew. Chem., Int. Ed.* **2013**, *52*, 7143–7146. DOI: 10.1002/anie.201300129.
- [57] J. R. Garbow, D. P. Weitekamp, and A. Pines. Bilinear Rotation Decoupling of Homonuclear Scalar Interactions. *Chem. Phys. Lett.* **1982**, *93*, 504–509.
- [58] J. A. Aguilar, M. Nilsson, and G. A. Morris. Simple Proton Spectra from Complex Spin Systems: Pure Shift NMR Spectroscopy Using BIRD. *Angew. Chem., Int. Ed.* **2011**, *50*, 9716–9717. DOI: 10.1002/ange.201103789.
- [59] A. Lupulescu, G. L. Olsen, and L. Frydman. Toward single-shot pure-shift solution <sup>1</sup>H NMR by trains of BIRD-based homonuclear decoupling. *J. Magn. Reson.* **2012**, *218*, 141–146. DOI: 10.1016/j.jmr.2012.02.018.
- [60] M. Foroozandeh, R. W. Adams, N. J. Meharry, D. Jeannerat, M. Nilsson, and G. A. Morris. Ultrahigh-Resolution NMR Spectroscopy. *Angew. Chem., Int. Ed.* **2014**, *53*. DOI: 10.1002/anie.201404111.
- [61] J. Mauhart, S. Glanzer, P. Sakhaii, W. Bermel, and K. Zangger. Faster and cleaner real-time pure shift NMR experiments. *Journal of Magnetic Resonance* **2015**, submitted.
- [62] M. A. Smith, H. Hu, and A. J. Shaka. Improved Broadband Inversion Performance for NMR in Liquids. *J. Magn. Reson.* **2001**, *151*, 269–283. DOI: 10.1006/jmre.2001.2364.
- [63] P. Sakhaii, B. Haase, and W. Bermel. Experimental access to HSQC spectra decoupled in all frequency dimensions. *J. Magn. Reson.* **2009**, *199*, 192–198. DOI: 10.1016/j.jmr.2009.04.016.
- [64] P. Sakhaii, B. Haase, W. Bermel, R. Kerssebaum, G. E. Wagner, and K. Zangger. Broadband homodecoupled NMR spectroscopy with enhanced sensitivity. *J. Magn. Reson.* **2013**, *233*, 92–95. DOI: 10.1016/j.jmr.2013.05.008.
- [65] G. E. Wagner, P. Sakhaii, W. Bermel, and K. Zangger. Monitoring fast reactions by spatially-selective and frequency-shifted continuous NMR spectroscopy: application to rapid-injection protein unfolding. *Chem. Commun.* **2013**, *49*, 3155–3157. DOI: 10.1039/c3cc39107h.